Measurements to Understand the Flow Mechanisms Contributing to Tandem-Rotor Outwash

Manikandan Ramasamy　　　　Mark Potsdam

US Army Aviation Development Directorate —AFDD
Aviation & Missile Research, Development & Engineering Center
Research, Development & Engineering Command
Ames Research Center, Moffett Field, CA 94035

Gloria K. Yamauchi

Aeromechanics Office
NASA Ames Research Center
Moffett Field, CA 94035

Abstract

Downwash and outwash characteristics of a model-scale tandem-rotor system in the presence of the ground were analyzed by identifying and understanding the physical mechanisms contributing to the observed flow field behavior. A building block approach was followed in simplifying the problem, separating the effects of the fuselage, effects of one rotor on the other, etc. Flow field velocities were acquired in a vertical plane at four aircraft azimuths of a small-scale tandem rotor system using the particle image velocimetry (PIV) technique for radial distances up to 4 times the rotor diameter. Results were compared against full-scale CH-47D measurements. Excellent correlation was found between the small- and full-scale mean flow fields (after appropriate normalization using rotor and wall jet parameters). Following the scalability analysis, the effect of rotor height on the outwash was also studied. Close to the aircraft, an increase in rotor height above ground decreased the outwash velocity at all aircraft azimuths. However, farther away, the longitudinal and lateral axes of the aircraft showed increasing and decreasing outwash velocities, respectively, with increasing rotor height. Measurements also indicated the presence of large-scale (of the size of the rotor height) shear-layer vortical structures along the ground that could be the source of low-frequency (approximately 1 Hz) flow variation observed in the full-scale measurements. Flow visualization studies and PIV measurements were also made on jets of different sizes to complement the observations made on rotors wherever possible. Baseline rotor measurements were made out-of-ground effect to understand the nature of inflow distribution for realistic rotor configurations and their modified characteristics in the presence of ground. Lastly, a feasibility study on applying high-fidelity CFD simulations for outwash study was conducted using Helios to model an isolated rotor configuration IGE at full-scale Reynolds number. The results were encouraging and demonstrated the practical challenges associated with predicting rotor outwash.

Nomenclature

C_T	thrust coefficient
D	diameter of the rotor
h	rotor height above ground
r	radial distance from the aircraft reference center
V_h	hover induced velocity using momentum theory
V_r	component of velocity along the r-coordinate
V_z	component of velocity along the z-coordinate
z	coordinate normal to the ground (z=0 at ground)
$z_{1/2}$	wall jet half-height
z_r	coordinate normal to the rotor plane (z=0 at rotor plane)

Introduction

When hovering in proximity to the ground, downwash from an aircraft impinges on the ground and moves radially away from the aircraft. The outward moving high velocity air is often referred to as outwash. For some applications the outwash is used advantageously as in the case of frost prevention in orange orchards (Ref. 1). However, the drawbacks of helicopter outwash far outweigh the benefits. A summary of the adverse effects of downwash/outwash (DWOW) from a V/STOL aircraft for both civil and military situations was reported as early as 1967 (Ref. 2) and more recently in a comprehensive summary provided in Ref. 3.

Reference 2 comprises a wide range of full-scale rotor flow field measurements from conventional single main rotor helicopters, overlapping tandem rotor helicopters, and tilt wing aircraft. The disk loading of aircraft considered vary from 2.5 lb/ft² up to 50 lb/ft², producing max-
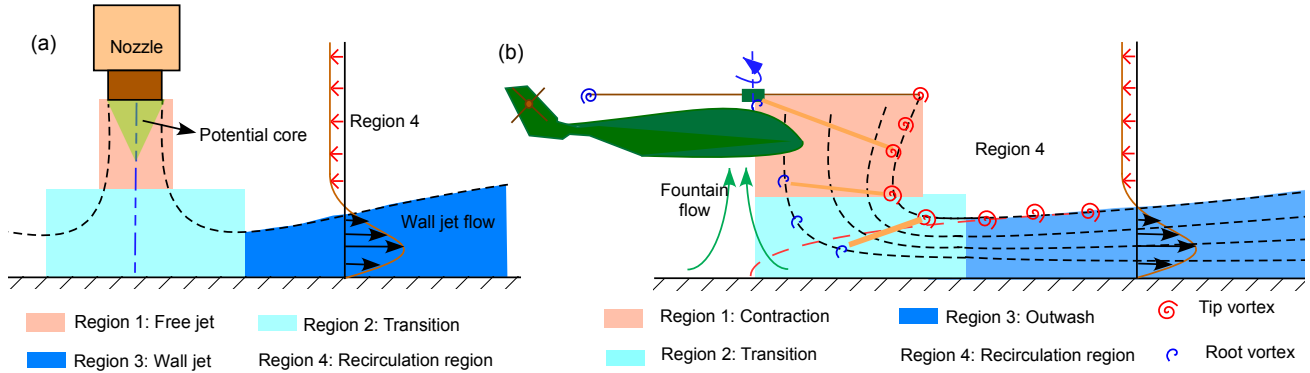
Figure 1: Regions of flow: (a) Impinging jet (b) Rotor in ground effect.

imum wind velocities of 25 kts to greater than 100 kts, respectively. Such high velocities have resulted in temporary blindness, excessive loss of heat or hypothermia, high fatigue, irrecoverable loss of balance for any approaching personnel, and toppling canvas tents pitched near the hovering zone. Secondary detrimental effects of high velocity rotor outwash include loose objects (for example, glass pieces, debris, rocks) acting as projectiles causing personnel injury.

Brownout and whiteout are significant problems when the DWOW lifts the sand/dust or snow from the ground to engulf the entire aircraft. Substantial effort has been invested in brownout investigations, including characterizing the effect of DWOW on the formation of particulate clouds, pilot visibility issues in brownout, dust entrainment into engine inlets, blade erosion, and increased aircraft maintenance.

Though almost 50 years old, the outwash velocities re-

Figure 2: Flow complexities in tilt and tandem rotors.

ported in Ref. 2 are consistent with the outwash of current day V/STOL aircraft (Ref. 3). Recent measurements on the CH-53E, MV-22 and CH-47D show peak outwash velocities as high as 95, 100 and 90 kts, respectively, with the adverse effects reported in Ref. 2 still applicable today. The limited knowledge of the behavior of rotor wakes in ground effect (IGE) poses a challenge for mitigating the problems caused by rotor outwash. Previous fundamental research on impinging jets (Refs. 4–6) and wall jets (Ref. 7) have so far provided the foundation for rotor DWOW analysis IGE. The justification to analyze rotor DWOW using an impinging jet formulation is explained by first describing the flow field similarities between a hovering rotor IGE and a jet impinging on a ground plane. Such a discussion leads to understanding the necessity for comprehensive flow field measurements on the tandem rotor configuration made in the present study.

Jets and Rotor Wakes

A rotor wake in hover out-of-ground effect (OGE) is comparable to a free jet flow, albeit with the obvious additional complexities arising from the presence of tip vortices, vortex sheets, and non-uniform inflow in the rotor wake. Far below the rotor plane, the downwash is expected to lose all influence of the geometric details of the rotor and resemble an axisymmetric jet (Ref. 8). Not much emphasis has been given to this analogy (rotor wake and free jet flow) because the rotor performance (or vibration or noise) is weakly dependent on the flow field far away from the rotor plane. On the other hand, the outwash velocities and their adverse effects are significant enough to warrant more attention in the far wake for a rotor operating IGE.

Downwash/outwash analyses for helicopters have benefitted from the research conducted on impinging jets and the resulting wall jet because of their similarity in flow development. Rotor height, diameter, and helicopter disk loading are analogous to the nozzle height, diameter, and
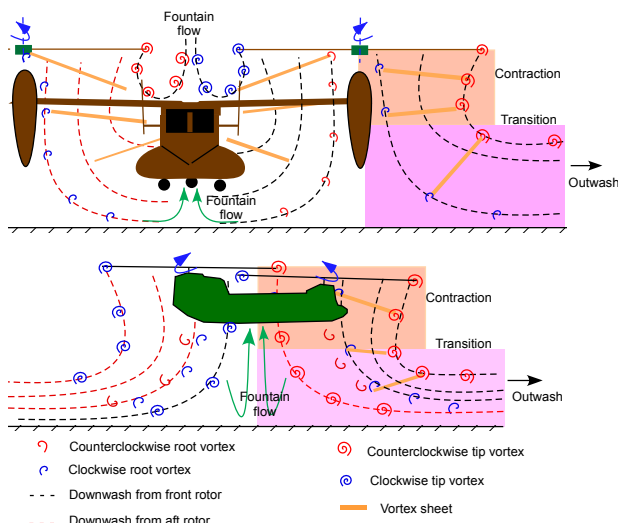
Reference	Type (Aircraft)	Scale/Diameter
Taylor, 1950 (Ref. 17)	S, C, Ta	20 in & 45 in
Fradenburgh, 1958 (Ref. 18)	S	24 in
Bolanovich & Marks, 1959 (Ref. 19)	S	75 ft
Bryan, 1960 (Ref. 20)	Ti(VZ-2)	28in & 9ft
Newsom &Tosti, 1962 (Ref. 21)	Ti(VZ-2, X-18)	1/4 to 1/8 scale
Harris, 1976 (Ref. 22)	S(CH-53E)	Full-scale
Light, 1989 (Ref. 23)	S	3.62 ft
Lake, 1998 (Ref. 24)	Ti(MV-22)	Full-scale
Wadcock, 2005 (Ref. 25)	V-22	1/40th scale
Wadcock, *et al*., 2008 (Ref. 26)	S(UH-60L)	Full-scale
Nathan & Green, 2008 (Ref. 27)	S	7 in
Johnson *et al*., 2009 (Ref. 14)	S	7 in
Lee *et al*., 2010 (Ref. 11)	S	6.7 in
Wong & Tanner, 2010 (Ref. 28)	S(EH60-L)	Full-scale
Milluzzo *et al*., 2010 (Ref. 29)	S	32 in
Milluzzo & Leishman, 2010 (Ref. 15)	S	32 in
Sydney & Leishman, 2011 (Ref. 30)	S	7 in & 32 in
Silva & Riser, 2011 (Ref. 31)	Ta(CH-47D)	Full-scale
Present study	Ta(CH-47D)	$1/56^{th}$ scale

Table 1: Past experiments on a rotor operating IGE (S=single, C=Coaxial, Ta=Tandem, Ti=Tilt).

nozzle exit pressure, respectively. Figure 1 shows the similarity in the analysis zones between impinging jets and rotors in ground effect.

Historically (Ref. 3), the entire DWOW analysis was divided into four regions (Fig. 1b) not for convenience but based on different kinds of flow mechanisms that dominate in each region. The four regions originated from impinging jet analysis. For example, Region 1 in the jet corresponds to a flow development zone where a potential core still exists. In the outer layer of the jet, shear layer vortex ring instabilities start transferring momentum from the center to the outer quiescent flow. Region 2 corresponds to the transition (impinging) region, where interaction with the ground turns the flow from an initial vertical direction to the horizontal direction along the ground. Region 3 is the wall jet region, where the peak value of radial velocity begins decaying (associated by increasing wall jet width) with increase in radial distance. Finally, Region 4 represents recirculation (induced flow by the jet).

In the case of rotors, wake contraction and downwash acceleration are dominant in Region 1. In the transition region, impingement of the rotor wake that turns the flow from the vertical to horizontal direction is key. The horizontal component of velocity (outwash) accelerates in this region. The third region, again similar to a jet, begins when the outwash velocity starts decaying with increase in radial distance. Region 4 is the recirculation region above the wall jet boundary. For a single rotor, the flow can be considered axisymmetric and the four regions are sufficient to represent all flow related calculations.

Experimental evidence supports the similarity between jet and rotor IGE flows. Increasing the rotor height (at least up to 2.5D above the ground) was found to increase the outwash velocity in the wall jet region (Refs. 9–11). A similar trend was observed by varying nozzle height in Refs. 4 and 12. Also, as expected, the effect of increasing disk loading of the helicopter (or the exit nozzle pressure for the jets) has been shown to increase the downwash/outwash velocities (Refs. 12, 13). The correlations found between the two flow fields, as well as the fundamental similarity in the flow development, justifies using jet analysis as a basis for rotor DWOW analysis.

Unlike single rotors, DWOW for multi-rotor configurations such as tilt- or tandem rotors is not axisymmetric because the radial flow away from the aircraft along their longitudinal axis is different from the lateral axis. Even within multi-rotors, the tilt-rotor offers a simpler flow field for DWOW analysis compared with tandem rotors. This is because tilt-rotor downwash/outwash along the lateral axis can still be analyzed using single rotor formulations because the outflow away from the starboard and port rotors from their respective shaft axes are independent of each other (see Fig. 2). Along the longitudinal axis, where the flow from both rotors merge, axisymmetric impinging jet analysis is not applicable. However, fundamental research on twin-jets operating in proximity to each other (Ref. 12) provide the necessary foundation for tilt rotor analysis.

An overlapping tandem rotor system presents a unique case. Combined with the challenges along the lateral axis

(starboard-port), even the flow along the longitudinal axis (forward-aft) is not simple. The flow from the forward rotor can be expected to affect the radial flow away from the aft rotor and vice versa – see Fig. 2. In essence, the radial outflow from all four sides of the aircraft have contributions from both rotors, questioning the applicability of jet analysis. Furthermore, unlike the tilt rotor, a tandem rotor configuration lacks an equivalent jet configuration.

Evolution of Downwash/Outwash Research

Early research on downwash/outwash (DWOW) was aimed at finding solutions for improving personnel safety as well as to mitigate brownout. Brownout needs additional understanding of the science of particulate transport (Refs. 5, 13–15). Often, measurements and analyses were conducted that complemented both DWOW and brownout.

Developing a scientific approach towards alleviating the adverse effects of DWOW begins with characterizing the overall flow field, i.e., establishing flow velocities around all configurations of aircraft at various heights from the ground and at various distances from the aircraft. Aircraft parameters such as gross weight, rotor disk loading, rotor height above the ground, blade loading distribution, number of blades, number of rotors, relative position of the rotors (in case of multi-rotor configurations) are all expected to affect the DWOW flow velocities. To understand the influence of the aforementioned parameters on DWOW, modeling and experimental efforts began more than five decades ago (Refs. 16–18). Since then, numerous experiments have been conducted on model-scale and full scale rotors IGE covering a wide range of rotor configurations including single, coaxial, tandem, tilt-rotor, and tilting aircraft. Table 1 represents the majority of the flow field measurements made on a hovering rotorcraft in ground effect.

Following Knight & Hefner's work (Ref. 16), Heyson (Ref. 32) used linearized vortex theory to predict rotor wake behavior in ground effect. The assumptions made in those models are not fully representative of rotor flow conditions, yet were simple enough to predict velocities with reasonable accuracy. George *et al*. (Ref. 13) used momentum-based models to quickly evaluate various rotor configurations. The model reported by George *et al*. was an assemblage of various models (that are associated with various regions shown in Fig. 1, as well as the region above the rotor) developed at different research facilities for different flow conditions and were later optimized for a rotor flow field. For example, to predict the peak flow velocities in Region 3 (Fig. 1b), George *et al*. used the wall jet theory proposed by Glauert (Ref. 7) and Ludwig (Ref. 4). The differences between the wall jet flow and the rotor outwash were accommodated by changing the values of peak velocity decay coefficients in the wall jet model using rotor measurements from Ref. 33. The sophistication of the model can be understood from the correction to the induced velocity within the formulation to account for IGE, where the induced velocity will be lower than OGE values to produce the same rotor thrust. The ability to predict the DWOW characteristics around a side-by-side rotor, such as the tilt rotor, was achieved by applying an empirical correction to the estimated velocities along the longitudinal plane using data from Ref. 21. The limited availability of experimental data was the biggest drawback of the George *et al*. model. The model could not be validated beyond datasets that were used to derive several empirical coefficients within the model. One of the key shortcomings of the model is that the wake contraction expected in the downwash of the rotor was not accounted for, thereby reducing the number of flow regions to 3 in Fig. 1b (Regions 1 and 2 were analyzed together).

Ferguson (Ref. 34), in a series of reports, significantly improved the George *et al*. model by focusing on flow regions that are more relevant to personnel safety/brownout situations. One of the key features in the new model, referred to as RotWash, accounted for wake contraction. A separate flow model was developed to represent the flow in the transition region (Region 2) shown in Fig. 1b. Additional improvements were incorporated into RotWash, made possible from an increased number of available measurements (Refs. 12, 35–37) on jet and V/STOL outwash flows. RotWash also included additional rotor parameters such as the inclination of the rotor shaft (during takeoff and landing) and shipboard landing scenarios (i.e., with a free stream velocity resulting in a ground vortex).

Around the same time RotWash was being developed, Velkoff and Preston (Refs. 38, 39) proposed a similar momentum based model. Again, jet flow analyses were used as a basis for the model. Coefficients were chosen such that the decay of the peak mean outwash velocity is the slowest based on all the available measurements. The conservative choice was made in order to predict the worst-case outwash scenario (highest velocity) possible. A unique aspect of Preston's model is the capability to estimate DWOW from an open rotor (typical main rotor) and an enclosed rotor (e.g., Fenestron or ducted fan/propeller). For side-by-side rotor configurations, the velocity along the rotor-rotor interaction plane was assumed to be uniform and parallel to the ground (that is, the flow did not possess a wall-jet like velocity profile).

Recently, Preston and Ferguson combined their momentum-based mathematical models (Ref. 3). The newly developed model, RoWFoot, provides the DWOW footprint for any rotorcraft, overlapping and non-overlapping rotors. RoWFoot is by far the most comprehensive momentum-based DWOW prediction code currently available.

Preston et. al., (Ref. 3) recommend that complementing existing full-scale databases using high-fidelity computations is essential. One of the goals of the present work is to conduct a feasibility study to evaluate the applicability of a CFD simulation (Helios) to develop such a data set. A high-fidelity prediction should be validated with available measurements. A brief overview of computational work studying outwash is provided next.

There has been limited research on DWOW using high-fidelity computational methods. As with experiments, simulations were developed with both outwash and brownout mitigation as their goals. The most successful have employed the vorticity-velocity formulation of the Navier-Stokes equations (conservation variables are used here) without ground boundary layer modeling. Phillips *et al*. (Ref. 40) used VTM (Vorticity Transport Model) to model the brownout problem on a small-scale rotor (Ref. 41) with a blade element rotor model and uniform meshes for the wake with an inviscid (image) ground plane. Zhao & He (Ref. 42) used VPM (Viscous Vortex Particle Method), a particle method with a blade element rotor model, to successfully model the outwash of the small-scale rotor, CH-53E, and XV-15. Although a viscous ground plane boundary condition showed improved results over the inviscid ground results especially in forward flight, the ground boundary layer was not modeled.

Unpublished results by Hayden & Abras (Ref. 43) under the CREATE-AV (TM) program used Helios to model the outwash of the CH-53E. Good agreement with full-scale mean and maximum velocity measurements was obtained as long as a viscous ground was modeled. However, in spite of employing a no-slip ground boundary condition, the off-body Cartesian solver was used exclusively away from the unstructured blade meshes and, therefore, did not model the ground boundary layer. Both actuator disk and discrete blade modeling were used. As in the current work, Ref. 43 simulations required many rotor revolutions and the starting vortex was never ejected from the calculation. Adaption using the non-dimensionalized Q-criterion created approximately 1 billion grid points.

Thomas *et al*. (Ref. 41) used a conservative variable formulation in OVERTURNS to model a small-scale brownout experimental set up. Velocity profiles, wake trajectories, and qualitative visualizations were in good agreement with measurements and the physics of brownout and particle behavior were investigated. Polsky & Wilkinson (Ref. 44) used Cobalt, also a conservative variable formulation, with actuator disk and various turbulence models to study outwash near a hangar wall. Wadcock *et al*. (Ref. 26) showed near-field (within 1R) CFD results below the rotor of a UH-60A using OVERFLOW and ROT3DC. Numerous other calculations of DWOW and brownout have been performed with lower-order free wake methods and image planes (Refs. 45, 46). Never-

theless, applying CFD for outwash prediction is still an ongoing research area that requires methodical evaluation of boundary conditions, grid resolution, etc.

The present study evaluates whether inexpensive small-scale measurements are an adequate alternative to high-fidelity simulations and full-scale tests.

Technical Approach

In general, developing a semi-empirical model to accurately predict the outwash velocities of any rotor configuration depends on the predictive accuracies of the model upstream of the wall jet, i.e., in the contraction and transition regions. RoWFoot (Ref. 3) formulation agrees with this approach. However, the complexities in the rotor wake (i.e., blade tip and root vortices, vortex sheets, pulsing in the flow from the presence of blades, non-uniform downwash, and wake contraction) makes the downwash prediction a formidable task even today.

In the case of the CH-47D, downwash below the overlapping rotors introduces even more challenges because of the presence of twice the number of tip and root vortices compared to the aircraft longitudinal axis and their non-linear interactions with each other (e.g., merging). Such a complex downwash flow field is difficult to model, and even more difficult to validate because of the lack of downwash measurements for the CH-47D. One of the primary goals of the present work is to conduct a series of experiments to develop a high-fidelity data set that allows improved understanding of overlapping tandem rotor downwash in the presence of the ground, and that allows validation of computational predictions.

Lastly, as mentioned earlier, existing momentum-based models that are used to predict rotor DWOW are based on a jet analogy. Retaining the jet formulation while modifying the coefficients within the model are the primary approaches followed to introduce rotor wake complexities into the jet analysis. This approach is acceptable for estimating the mean characteristics of DWOW. However, to estimate the unsteady, high velocity fluctuations (gusts) in rotor outwash (as reported in Refs. 22, 24, 31), no flow model exists. For example, recent measurements (Ref. 31) from a full-scale CH-47D aircraft reported peak velocity values as high as 150% of mean velocities and unexplained low frequency fluctuations (of the order of 1 Hz) in the measured velocities, which suggest that the unsteady phenomena are not well understood. Basic unsteady flow analyses conducted on jets can aid our understanding, however. A need exists for high-fidelity measurements of steady and unsteady outwash velocities from a CH-47D rotor operating IGE in a controlled environment. As shown in Table 1, single rotor experiments and non-overlapping rotor (i.e., tiltrotors) experiments have been the main focus of DWOW

Description	Full-scale (Ref. 31)	Model-scale
Number of rotors	2	2
Blades per rotor	3	3
Rotor radius (in)	360	6.31
Rotor-Rotor distance (in)	470	8.33
Solidity	0.0849	0.057
RPM	225	3540
Tip speed (ft/s)	706.9	194.9
Aircraft gross weight or thrust (lb)	41,000	0.96
Disk loading (lb/ft^2)	7.25	0.042
Rotor rotation (fwd/aft)	CCW/CW	CCW/CW
Shaft tilt (deg, +fwd) – fwd/aft	9/4	2.5/0

Table 2: Aircraft Characteristics.

Figure 3: Model-scale tandem rotor system.

measurements. The full-scale CH-47D measurements by Silva and Riser (Ref. 31) represent the most comprehensive survey of the DWOW from a tandem rotor aircraft. Hence, the present work focused on conducting a series of model-scale measurements (see Fig. 3) to illuminate the steady/unsteady flow mechanisms contributing to the DWOW of a CH-47D.

The primary objectives of the study were: 1) acquire flow field measurements in a vertical plane, from the shaft axis out to 4 rotor diameters, at four aircraft azimuthal positions (forward, aft, starboard, and port) and compare mean DWOW velocities to the full-scale measurements from Silva and Riser (Ref. 31); (2) conduct a parametric study to understand the influence of one rotor on the other in terms of the outwash velocity, especially in front of and aft of the aircraft; (3) study the effect of the fuselage on the flow field; (4) acquire flow field measurements for a steady non-uniform impinging jet (at a similar scale as that of the model-scale rotor) and compare with single rotor and tandem rotor flow fields; (5) conduct simple ex-

periments using jets (at a Reynolds number similar to the model-scale rotor) to understand the unsteady flow phenomenon in the impinging jet/wall jet regions (Regions 2 and 3) that are expected to be present in rotor downwash/outwash, and (6) conduct feasibility studies using Helios to predict outwash for an isolated single rotor IGE and compare the flow field predictions with the model-scale measurements.

Description of Experiment

Figure 4 shows the set of experiments conducted in the present study. All the experiments were conducted in the U. S. Army hover chamber (25- by 25- by 30-ft high) at NASA Ames Research Center. The large testing volume ensured that flow recirculation effects were minimal.

Model aircraft The model aircraft (Fig. 3) represents an approximately 1/56th-scale CH-47D (Ref. 47, D=1.07ft). Table 2 provides the basic aircraft characteristics for the full-scale CH-47D and model-scale tandem-rotor aircraft. The radio-controlled aircraft model (Fig. 3) was post-mounted above a 2-piece ground plane. To simulate the hover configuration, the front rotor shaft was replaced with a longer shaft so that both rotors were at the same height above the ground plane, similar to the full-scale CH-47D hover configuration (see Fig. 9 of Ref. 31). For the model aircraft, the shaft angles of the forward and aft rotors were 2.5 deg (forward tilt) and 0 deg, respectively. Using the simplified hover trim attitude described in Ref. 31, the shaft angles of the full-scale CH-47D were estimated as 2.3 deg (forward tilt) and 2.5 deg (aft tilt) for the forward and aft rotors, respectively.

A load cell, shown in Fig. 3, was sandwiched between two plates and mounted in line with each rotor. The width of the two plates was less than the width of the fuselage so did not add to the blockage of the fuselage. The target aircraft C_T was achieved by insuring equal thrust-sharing between the two rotors. Thrust sharing for the full-scale

Description	PIV plane	h/D	Kind
Isolated rotor OGE	Axisymmetric	-	TH
Isolated rotor IGE	Axisymmetric	0.578	PL & TH
Single rotor w/ fuselage	Forward	0.578	PL
Tandem rotor	Forward, Aft, Starboard, Port	0.578, 1.0	PL & TH
Small nozzle	Axisymmetric	0.578	TH & FV
Small nozzle OGE	Axisymmetric	-	TH & FV
Large nozzle	Axisymmetric	0.578	TH
Large nozzle OGE	Axisymmetric	-	TH

Table 3: Details of measurements conducted in this study (TH=Time history, PL=Phase locked, FV=Flow visualization).

(a) Free jet, D=0.393 in   (b) Impinging jet, D=0.393 in, h/D=1.5   (c) Free jet, D=8 in   (d) Impinging jet, D= 8 in, h/D=0.57

(e) Isolated single rotor   (f) Single rotor IGE, h/D=0.57   (g) Single rotor IGE w/ fuselage, h/D=0.57

(h) Tandem rotor IGE, h/D=0.57 & 1

Figure 4: Set of experiments conducted in this study.

aircraft was a function of the aircraft CG location. The

Figure 5: Coordinate system and reference locations for outwash study.

forward rotor of the full-scale aircraft was computed to carry approximately 10% more thrust than the aft rotor. Since the laser sheet and cameras remained stationary, the post-mount, with model attached, was rotated to acquire flow measurements at 4 aircraft survey azimuths: 0 deg (forward of aircraft), 90 deg (starboard), 180 deg (aft of aircraft), and 270 deg (port). Figure 5 shows the coordinate system and reference locations for the flow field measurements presented in this study.

To evaluate the differences in the flow field between one rotor and two overlapping rotors, the front rotor was removed and flow measurements acquired for 180 deg aircraft azimuth. The flow field of an isolated rotor in ground effect without fuselage effects was acquired by removing the front rotor and fuselage, inverting the aircraft above the ground plane, and reversing the direction of thrust.

PIV System Figure 6 shows the three 16-MP cameras viewing the laser sheet orthogonally. Each camera viewed a region of interest (ROI) approximately 18-in wide with an overlap of about 2-in between camera ROIs. A single calibration target (800-mm high by 1000-mm wide) was
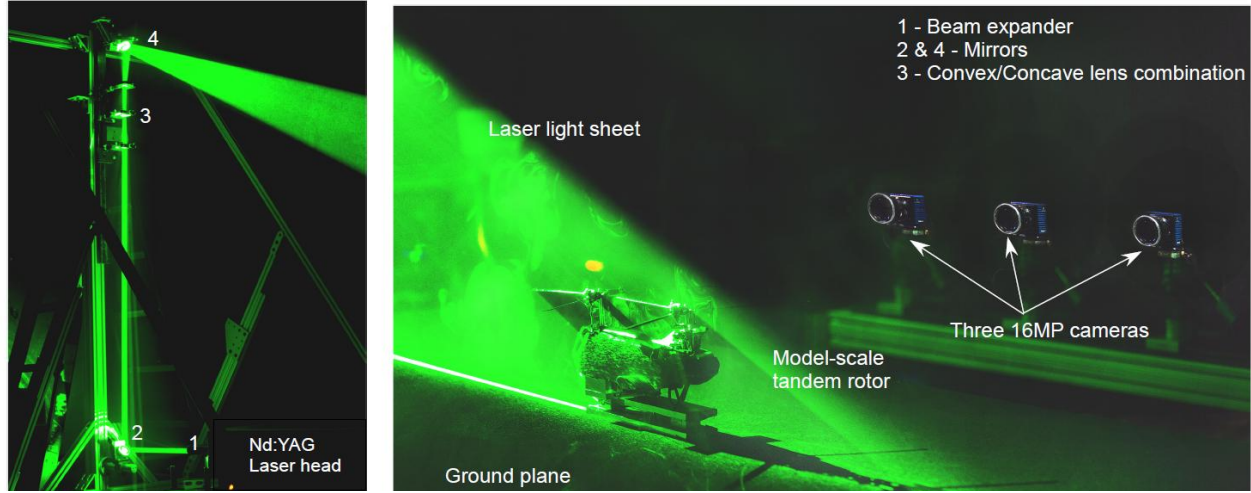
Figure 6: Experimental set up.

used to calibrate all 3 cameras simultaneously.

PIV images were acquired in two modes: phase-locked with the rotor and free-run. DaVis 8.1.3 was used to acquire the 2-D PIV images simultaneously from the 3 cameras. In phase-locked mode, 100 images were acquired at 0.22 Hz. In free-run, 500 images were acquired at 0.49 Hz. Only free-run results are shown in this study. The aircraft C_T was maintained at approximately $C_T = 0.0061$ (equal thrust on both rotors, equivalent to 41,000 lb full-scale CH-47D) and rotor RPM = 3540 (V_{tip}=195 ft/s) for all test conditions. Measurements on steady jets of two different nozzle diameters were also made: (1) D=0.393 in and (2) D=8 in. The larger nozzle produced non-uniform flow (similar to that of Ref. 4), equivalent to a single rotor with high tip loading. The nozzle experiments were conducted both OGE and IGE.

CFD – Helios

Helios (HELIcopter Overset Simulations) is the rotary-wing product of the US Army and CREATE-AV (TM) (Air Vehicles) program sponsored by the DoD High Performance Computing Modernization Office (Ref. 48). Helios uses an innovative multi-mesh paradigm with unstructured and/or structured meshes in the near-body surrounding the solid surfaces to capture the wall-bounded viscous effects and uniform Cartesian grids in the off-body to resolve the wake through a combination of higher-order algorithms and adaptive mesh refinement (AMR).The structured adaptive solver SAMARC is used for the Cartesian off-body region, between the rotor and the ground. SAMARC solves the inviscid Euler equations using a 5thorder spatial discretization scheme and 3rd-order explicit Runge-Kutta time integration scheme.

AMR capability in SAMARC enables the CFD to ac-

curately, efficiently, and automatically capture the features in unsteady flow based on non-dimensionalized Q-criterion. The Cartesian block-structured off-body system is automatically generated, refined, and de-refined around flow features such as tip vortices. The off-body grid is adapted frequently to allow fine regions of the off-body mesh to keep up with the moving surfaces and tip vortices. Also, NASAs OVERFLOW flow solver has recently been integrated into Helios (Ref. 49) that allows the use of the high-order, efficient, structured mesh algorithms in the near-body. For turbulence modeling, the 1-equation Spalart-Allmaras (SA) model is used with a fully turbulent assumption and an approximate rotation and curvature correction. The SA turbulence model was chosen in order to allow coupling with the same model in a viscous SAMARC solution, which is ongoing.

CFD predictions were made for the isolated rotor configuration, however, at full-scale Reynolds numbers. Operating conditions of the rotor were applied to replicate full-scale test conditions of Ref. 31. The blades were modeled with 3 curvilinear structured grids each (main blade, tip cap, and root cap) in OVERFLOW. The blades were rigid with specified collective, coning, and torque offset. An equivalent time step of 0.25 deg of rotor revolution was used.

Because the off-body solver only allows uniform Cartesian meshes, the viscous ground boundary layer was also fully modeled in OVERFLOW. A cylindrical mesh with viscous clustering in the normal direction was employed and extended 45 inches from the ground and to 8R. A no-slip boundary condition was used on the ground. In the radial direction out to about 2R and at the top boundary of the mesh the spacing matches the smallest spacing of
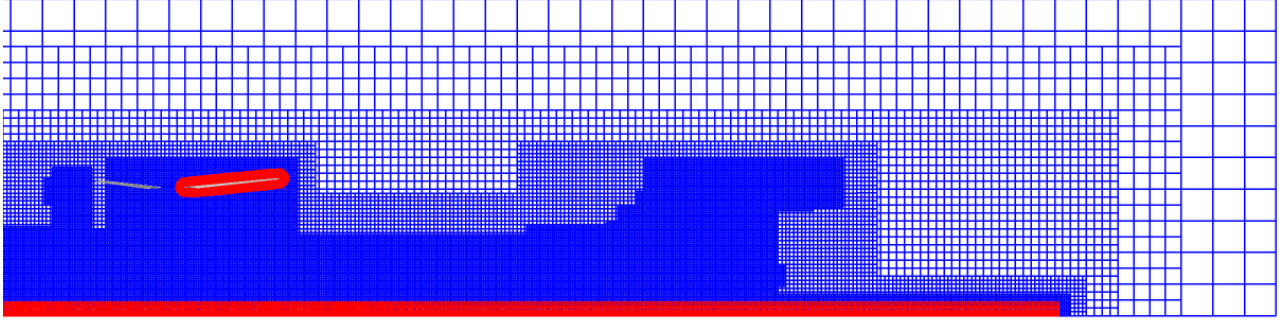
Figure 7: Helios dual-mesh modeling CH-47 blades (red), ground boundary layer (red) and AMR off-body (blue) (every other point shown).
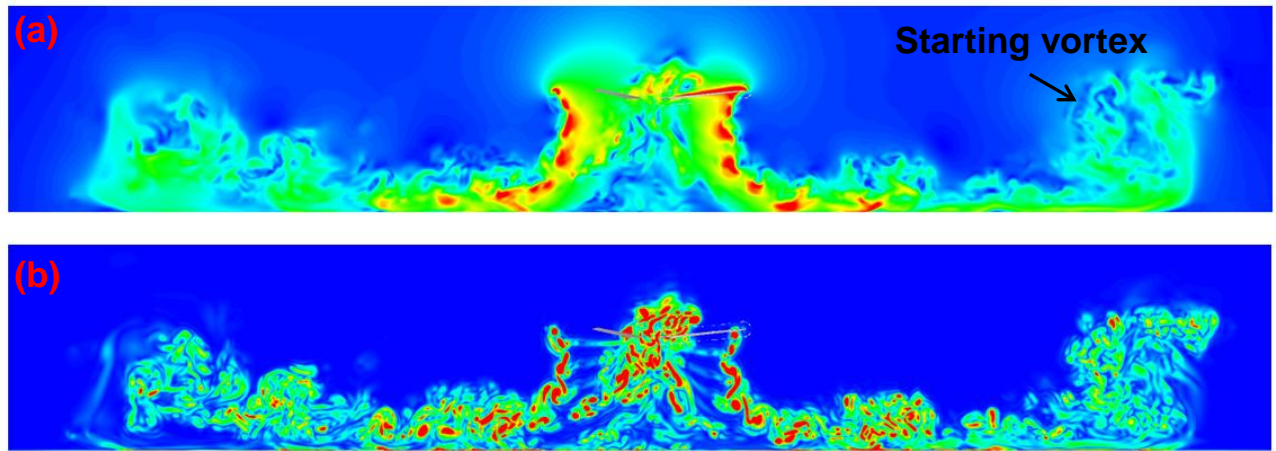

Figure 8: Helios instantaneous solution (a) velocity magnitude, (b) vorticity magnitude.
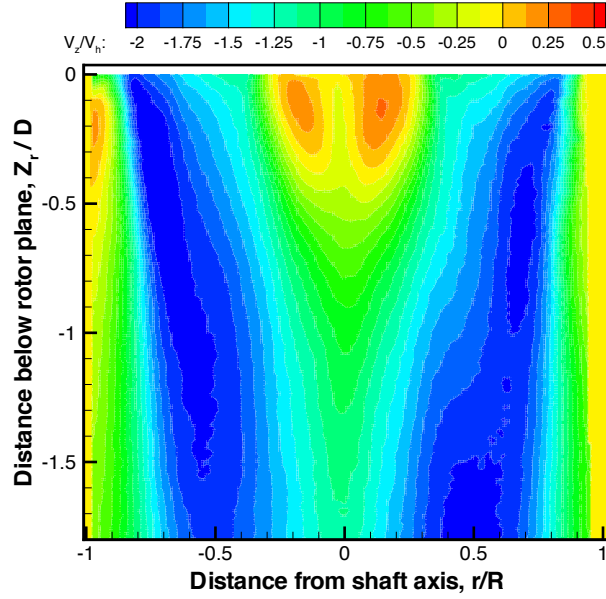
the SAMARC Cartesian mesh, 3.2 inches (approximately 10% of the rotor chord). The cylindrical ground boundary layer mesh is 427 (radial) x 361 (azimuthal) x 65 (normal). There are a total of 10.6 million grid points modeling the ground, while the rotor is comprised of 10.5 million grid points. Beyond 8R and out to 10R the off-body uniform Cartesian mesh is used with an incompatible spacing mismatch transitioning between the boundary layer grid and the off-body Cartesian near the ground. Extrapolation boundary conditions on the top and side planes of the Cartesian mesh allow for the necessary outflow. AMR is employed to capture the tip vortices and vortical interactions with the ground. Up to 450 million grid points are generated with AMR. A crossection of the mesh is shown in Fig. 7. The near-body OVERFLOW grids are in red, the off-body AMR grids are in blue.

The calculation is set up to model the test conditions at full-scale Reynolds number and tip Mach number, with the rotor hub center 34.3 feet above the ground. Thirty-five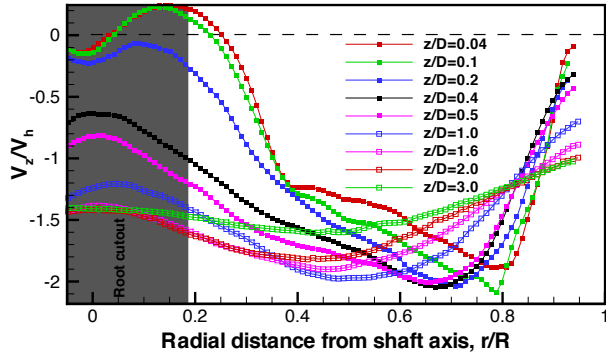 rotor revolutions were simulated. An initial 15 rotor revolutions were run without adaption on a coarse mesh in order to push the starting vortex away from the rotor. Even after 35 rotor revolutions the starting vortex is still in the calculation, and the wall jet has not reached beyond 5R. Outwash modeling with CFD is an expensive proposition. Many more rotor revolutions are needed in order to push the starting vortex out of the domain and obtain statistical calculations of the outwash velocities at all radial locations. In the current calculations, results are only available out to 4R and velocity calculations have been averaged over 20 rotor revolutions. Sample velocity and vorticity magnitude contours after 35 rotor revolutions are shown in Fig. 8.

Results

Baseline isolated single rotor measurements operating in hover out of ground effect will be discussed first. Following this, flow field measurements made in ground effect will be analyzed. Lastly, unsteady effects will be dis-

9

(a) Velocity contour

(b) Velocity profiles

Figure 9: Flow field of a isolated single rotor in hover (OGE).

Figure 10: Wake contraction and equivalent induced velocity ratio.

cussed using instantaneous PIV realizations along with complementary simple jet measurements. Each section has its own objective. However, the underlying goal that connects all the objectives is improvement in the fundamental understanding and characterization of tandem rotor system DWOW. Since limited full-scale data are available for validation, along with full-scale CH-47D measurements (Ref. 31), observations made in the past from single/multiple rotors both with and without a fuselage are compared against the present measurements wherever possible.

Isolated Single Rotor OGE

The objective of this measurement was to establish the baseline wake characteristics, specifically the downwash distribution, for a single isolated rotor in hover. The isolated rotor configuration was achieved by removing the front rotor blades and fuselage of the tandem rotor model,

thereby removing any effect of blade overlap on the inflow distribution. Also, the ground plane was removed and the model rotated so that the rotor axis was horizontal. The wake was therefore unimpeded for more than 15 rotor diameters. Establishing a baseline is necessary because existing DWOW models use simple momentum theory by assuming that the downwash accelerates to twice the inflow velocity measured at the rotor plane. In fact, introducing downwash acceleration is one of the key changes made to the jet analysis to represent rotor behavior. However, reality is far different from momentum theory assumptions in that the effects of a finite number of blades, tip vortices, and root cut-out play a substantial role in the resulting non-uniform inflow distribution. Accurate representation of the inflow distribution is the first step in downwash prediction.

Flow velocities measured for the isolated single rotor configuration are shown in Fig. 9. The color contour is the downwash velocity normalized using wake velocity scale $V_h = \sqrt{T/2\rho A}$. Corresponding downwash velocity profiles at various downstream distances are shown in Fig. 9b. At the center, even though the rotor operated out of ground effect, flow recirculation occurred below the non-lifting portion of the blade, i.e., at the root cut out. Recirculation was continuously energized by the blade root vortex that transferred momentum from the downwash velocity.

Although the root cut out is only 10% of the rotor diameter, the region of recirculation covers about 0.26D of the rotor disc in the near wake (at about 0.04D below the rotor) and gradually reduces with increasing vertical distance before disappearing at about 0.2D below the rotor. Nevertheless, the center of the rotor still had low momentum flow; consequently, viscous shear continuously transferred momentum from the accelerating downwash velocity to the low-momentum region. The result of the transfer of momentum is evident in the velocity profiles of Fig. 9b. The velocity deficit near the center of the rotor

10

gradually reduced with increasing z/D. At z/D=3, down-wash velocity is almost uniform across the rotor disc. As Spalart (Ref. 8) suggested, at even greater downstream distances, the rotor wake may begin behaving like a jet with maximum velocity found near the center rather than at the edges.

To compare momentum theory against a realistic rotor that has non-uniform inflow (as in the present study), the slip stream boundary, as defined by the location of the tip vortices, must be identified. However, often 1R below the rotor, the tip vortices interact and merge with each other leaving no clear distinction of the slipstream boundary, making the comparison with momentum theory a challenge. An alternative method for such situations is described here.

To be consistent over the entire downstream distance, and for the lack of a better alternative, the location of the peak downwash velocity was chosen as the slipstream boundary. In the near wake, this corresponds to the location of the tip vortex measured from the shaft axis minus the radius of the tip vortex core. Figure 10 shows the locus of peak downwash velocity that identifies the slip stream boundary and wake contraction. The non-uniform inflow also poses a problem in that an equivalent induced velocity needs to be estimated. In the present study, the induced velocity was estimated by finding the average of the downwash velocity from the shaft axis to the peak V_z at all distances below the rotor. The estimated equivalent induced velocity normalized by the V_h is shown in Fig. 10. At $z_r/D=0$ the value is less than 1 probably because of the upwash resulting from the recirculation. At a distance of about 1 diameter beneath the rotor plane, the downwash velocity reaches its peak of about 1.5 times the hover induced velocity, much less than the factor of 2 expected from momentum theory. From 1 diameter to 3 diameters, the equivalent average induced velocity remains nearly constant with a very slow reduction in magnitude.

Results from the alternative approach suggests that the downwash acceleration does not result in $2V_h$ even far below the rotor ($z_r/D>3$). While such deviation from momentum theory based on uniform loading is expected for a realistic rotor with non-uniform loading, quantifying the increase in downwash velocity will be useful for developing semi-empirical models.

In Ground Effect

Having established the downwash distribution beneath the rotor in hover OGE, the next step is to understand and characterize the DWOW of a tandem rotor system in ground effect.

A tandem rotor system with overlapping blades is unique in that the flow characteristics vary around the aircraft azimuth. Any effort to understand the DWOW of the tandem rotor system should begin with quantifying the influence of one rotor on the other. In this model-scale experiment the influence was discerned by simply removing the blades from either the front or the aft rotor. In addition, the fuselage was removable which allowed studies on an isolated rotor IGE to be conducted. Such a building-block approach was essential for understanding the flow mechanisms contributing to the DWOW behavior of a rotor system with overlapping rotors.

Figure 11 shows a time-averaged flow field for the forward rotor of the tandem rotor system in ground effect over the entire measurement distance. Similar results were obtained for all rotor configurations and azimuths listed in Table 3. The chosen color contour in Fig. 11 (angularity) clearly distinguishes three regions (see Fig. 1b) of analysis conducted in this study, i.e., (1) Contraction (Region 1); Transition (Region 2), and Outwash (Region 3). Region 4 of the image corresponds to the recirculation zone ($V_r < 0$, flow direction towards the rotor), and is not analyzed in this study.

For each Region, the following topics are explored:

1. IGE vs. OGE for isolated single rotors

2. Effects of the fuselage for rotor IGE

3. Single versus multi-rotors (or the effects of aft rotor on the front rotor and vice versa), IGE

4. Differences in the DWOW between the longitudinal and lateral axis of the tandem rotor IGE, and

5. Effects of rotor height on DWOW, IGE

Unless specifically mentioned, all measurements correspond to IGE operating conditions for all rotor configurations. Results along longitudinal axis will be discussed first before lateral axis in all the following discussions.

Region 1: Contraction

Taking into account the average rotor height for an Army helicopter with wheels-on-ground and the height of an average person operating in close proximity to the helicopter, velocities measured in the transition and outwash region are more critical than the contraction region. However, from a modeling perspective, Region 1 is very important because the flow in Regions 2 and 3 depend on the nature of flow in Region 1. The objectives of this section are to: (1) define the boundary between Regions 1 and 2. For this study, the boundary is defined as the location of maximum wake contraction (or highest downwash velocity); and (2) understand and characterize the downwash flow field below the rotor disk in Region 1 for various rotor configurations IGE and their deviations from OGE.

Time-averaged downwash velocities from an isolated single rotor, a single rotor with fuselage, and the tandem
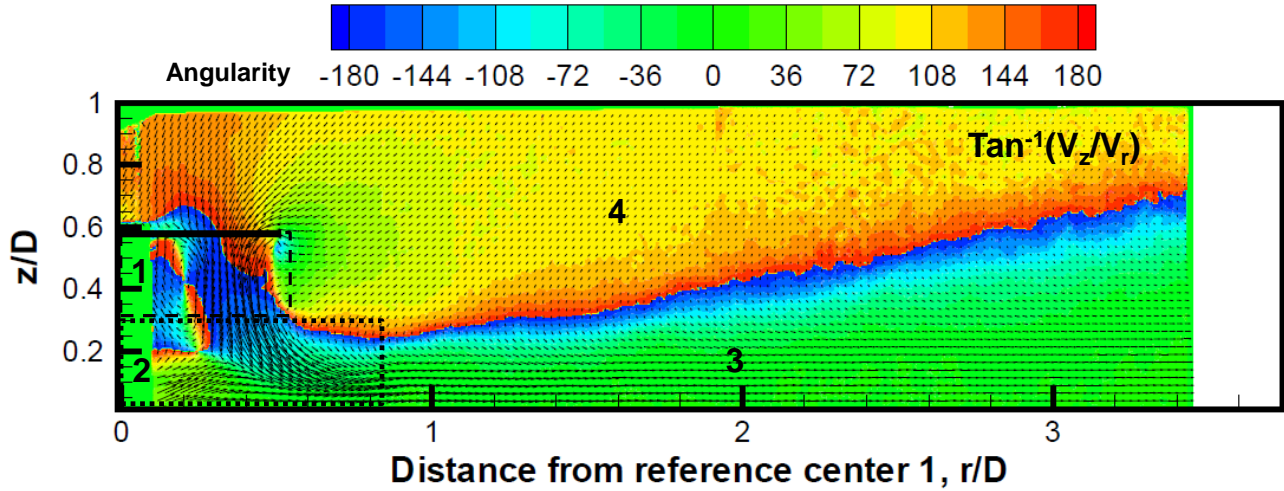
Figure 11: Time averaged flow field of tandem rotor IGE (forward rotor, h/D=0.578).

rotor system are shown in Fig.12 for a rotor height (h/D) of 0.578. In the case of the tandem rotor system, velocities from both the front and aft rotors are shown. Streamtraces are drawn to highlight important features present in the flow field.

The first step is to identify the location of maximum wake contraction to distinguish Region 1 and 2 in Fig. 11. The challenge becomes immediately obvious because of the absence of a defined parameter such as the tip vortex trajectory. So, an unconventional however logical approach is followed. Downwash velocity accelerates to its maximum value at the point of maximum wake contraction; its location can be identified by plotting the profiles of downwash velocity measured along a vertical cut (normal to the ground). Remember, downwash is usually studied using planes that are parallel to the rotor plane and not using vertical cuts. Here, vertical cuts are used to identify the location of maximum wake contraction. Nevertheless, the results from vertical cuts should be consistent with planes parallel to the rotor plane as long as the cut is inside the "slipstream" boundary. Figure 13 shows the downwash velocity distribution at three different radial stations for the isolated rotor case in ground effect. As, expected the maximum downwash velocity occurred at the same z/D ($\approx$0.44) for all three cuts.

Figure 14 shows the velocity profiles for all rotor configurations IGE at a radial station of 75% blade span. In the case of the isolated single rotor, the maximum contraction was observed at 17%D below the rotor plane. This location moved closer to rotor (16%) in the presence of the fuselage. The front and aft rotors of the tandem rotor system configuration also showed maximum wake contraction at around 17%D below the rotor. This can also be confirmed through the streamtraces from the tip shown in Fig. 15, where maximum contraction appears to occur around z/D=0.45.

Figure 14 also includes isolated single rotor measurements OGE to compare against IGE cases. In ground effect, the rotors require less power to produce the same thrust (thrust augmentation). Figure 14 confirms that the downwash velocities for all rotor configurations IGE measured across the disc were lower than the OGE case. The source of the reduced power comes from the reduction in the induced velocity. Among the IGE configurations tested, the rotor with fuselage showed lower downwash velocity than the isolated rotor despite the adverse download caused by the presence of the fuselage that required rotors to produce more thrust (to match the same C_T as isolated rotors). Comparing the front and aft rotors, the front rotor showed slightly lower downwash velocity than the aft rotor because of the slight inclination of the front rotor shaft (see Table 2) that produced velocity vectors at an angle (of the order of 3 deg).

Having established the location of the waist (17%D below the rotor) of the contracting wake, Figs. 16a and b show the vertical and horizontal components of the velocities made at the waist location across the rotor disc for various rotor configurations. The changes to the inflow distribution are compared against the isolated single rotor operating OGE.

Figure 16a confirms the findings from Fig. 14 i.e., all rotor configurations operating IGE produced less downwash velocity than the isolated rotor operating OGE (inside the wake boundary that is identified from the change in V_z slope near r/D=0.4). Recirculation found near the blade root gained strength IGE resulting in higher upwash velocities. For the isolated rotor, the presence of the ground also appeared to have pushed the center of recirculation radially outward from the shaft axis. Comparing downwash velocities with and without fuselage, the fuselage pushed the region of recirculation even further outward (Fig. 16) with slightly higher upwash velocities.
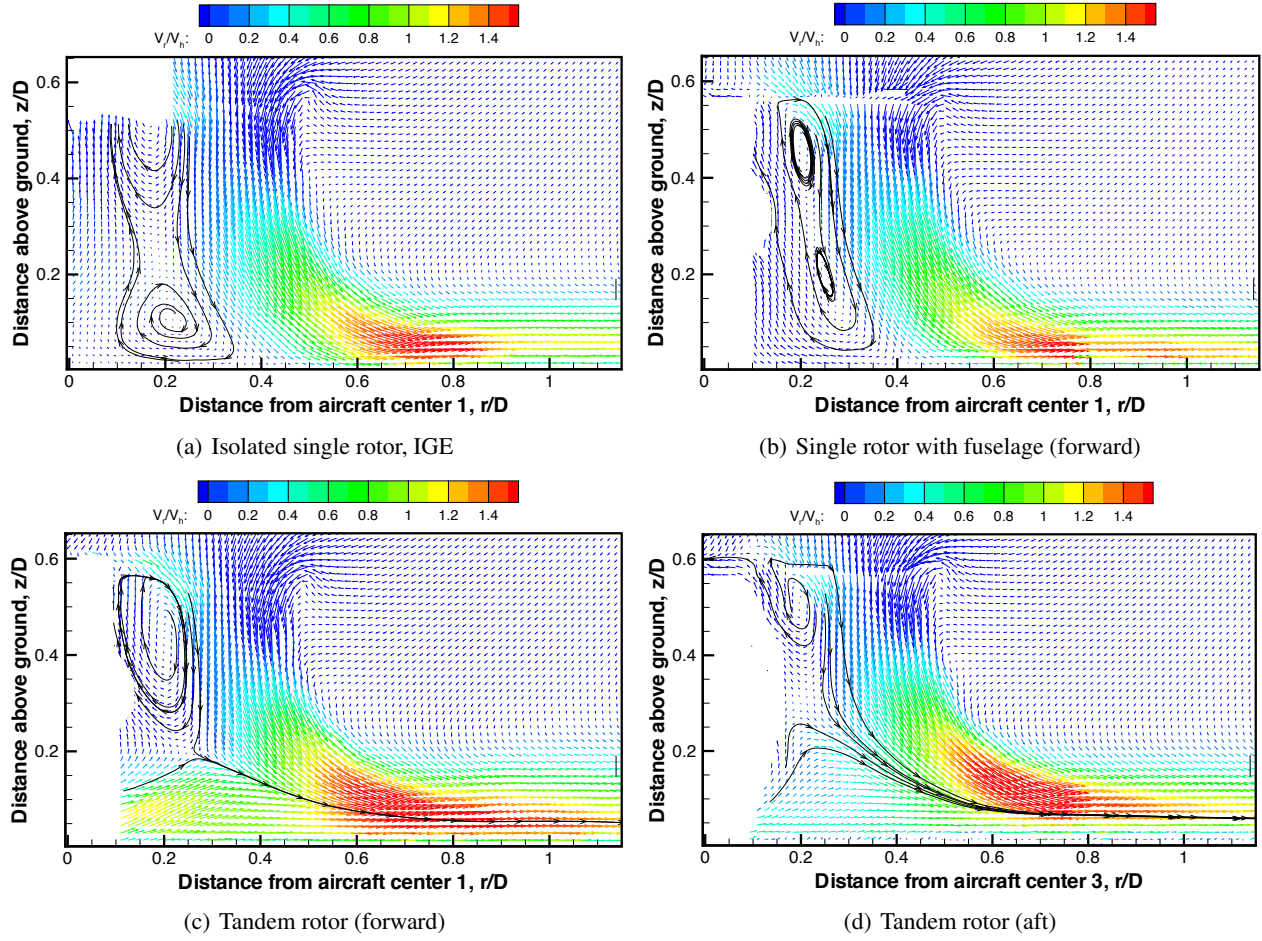
(a) Isolated single rotor, IGE

(b) Single rotor with fuselage (forward)

(c) Tandem rotor (forward)

(d) Tandem rotor (aft)
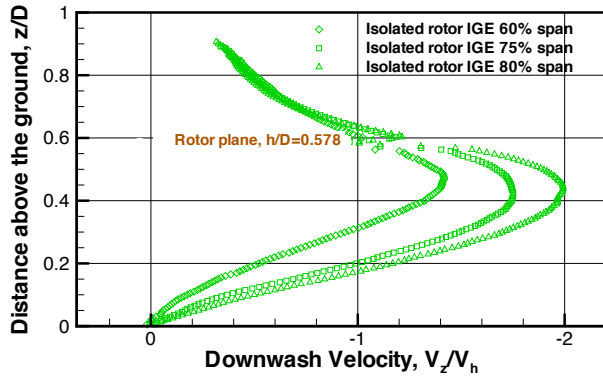
Figure 12: Flow field comparison at h/D=0.578.

Figure 13: Downwash velocity profiles at various blade span locations for isolated rotor IGE (h/D=0.578).
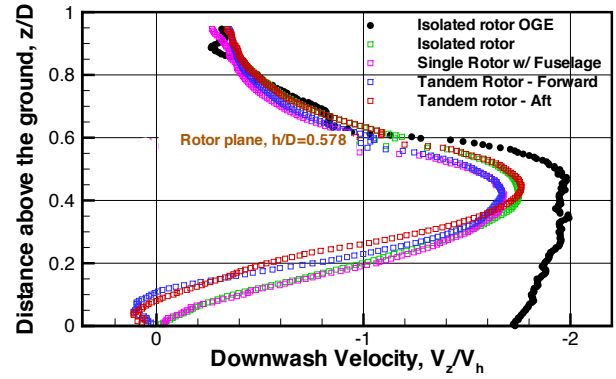

Figure 14: Variation of downwash velocity at 75% blade span normal to the rotor plane (h/D=0.578).

Figure 16a shows that the maximum downwash velocity occurs over a small region for any rotor configuration operating IGE, and is about $2 \times V_h$. This suggests that the average downwash beneath the rotor will be substantially lower than what is expected based on momentum theory.

Figure 16a also shows the CFD result for comparison.

Outboard, it is seen that the peak downwash velocity is lower by about 20%, the wake is slightly less contracted, and the wake slipstream boundary is noticeably wider. In the inboard region there is less upwash. Figure 8 confirms the existence of vortical flow which rises above the plane of the rotor indicating that there is upwash in the
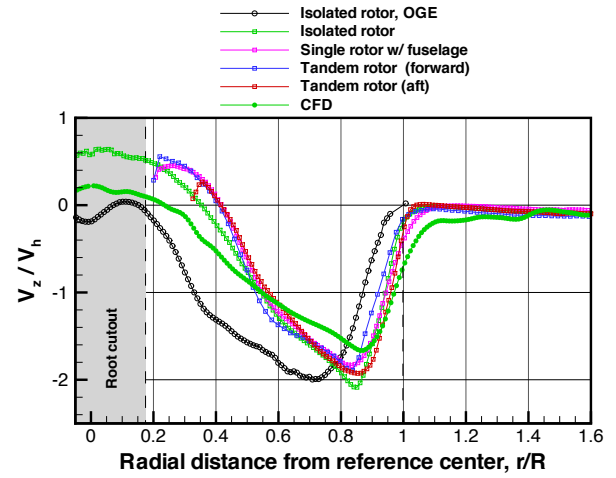
Figure 15: Streamtraces from two blade span locations for various rotor configurations (h/D=0.578).

root region due to the root vortices and the effect of the ground. The experimental and CFD simulation have different modeling of the hub, which is absent in CFD, and root cut-outs, which are tapered in CFD. These geometric differences may play a role in the inboard flow field. Overall, it appears that the momentum across the wake is similar, albeit with rather different radial distributions.
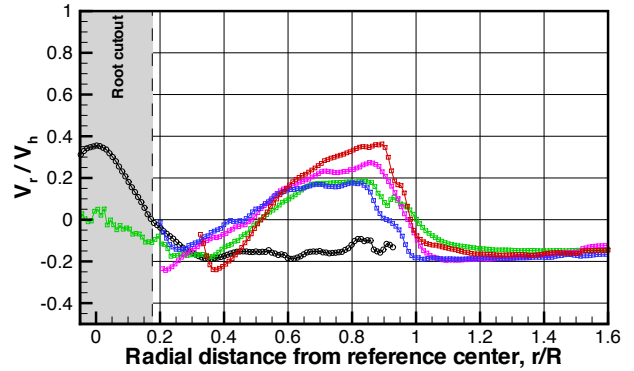
Figure 16b shows the horizontal component of the downwash velocity beneath the rotor disc for all rotor configurations. As the radial distances decrease from r/R=1.6 towards the shaft axis, V_r is negative indicating the flow is towards the rotor. This suggests that, in the case of brownout analysis, any particulate cloud formed beyond 1D will still be influenced by the induced velocity of the rotor, pulling the sand/dust towards the rotor. When r/R reduces below 1.0 (tip of the rotor blade), the slope changes twice before reaching the shaft axis that correspond to the wake boundary and the edge of the recirculation region shown in Fig. 12.

Figure 17a shows tandem rotor system downwash velocity comparison (normal cut at 75% blade span) for the front rotor for two different rotor heights (h/D=0.578 and 1.0). For h/D=1, the rotor plane was positioned 1D above the ground plane. Two key observations are: (1) increasing the hovering height of the rotor increases the maximum measured downwash velocity; and (2) the waist of the contracting wake occurs near 30%D below the rotor at higher hovering distance when compared with 17% at lower heights. However, when normalized with the rotor height above the ground (see Fig. 17b), the location of maximum downwash velocity is approximately 30% of rotor height (z/h=0.7) below the rotor plane for both cases.

Vertical velocity profiles extracted from horizontal cuts through the front rotor flow field are shown for two different rotor heights in Fig. 18. For the case of h/D=1, horizontal cuts were made at two locations below the rotor, z/D=0.44 and z/D=0.66, corresponding to the location of maximum downwash velocity for h/D=0.578 and
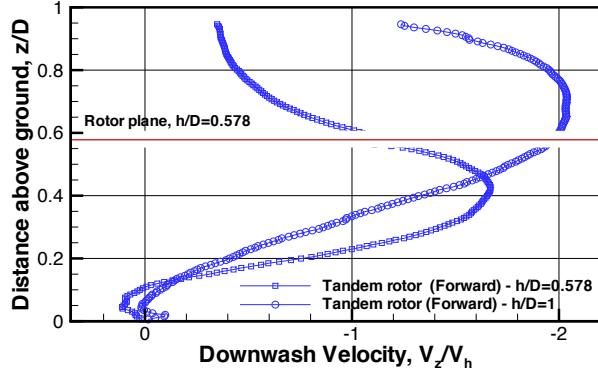

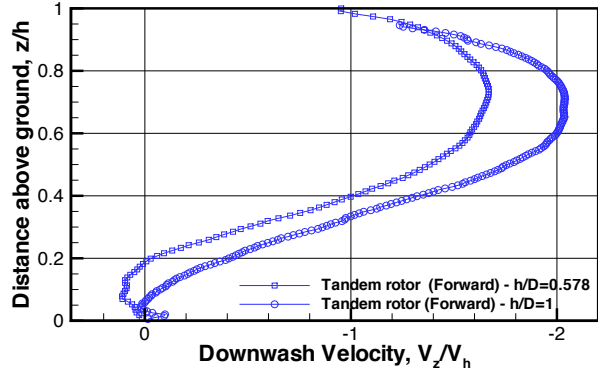
(a) Downwash velocity

(b) Horizontal velocity component

Figure 16: Velocity comparison below the rotor (at z/D=0.4) for various rotor configurations.

h/D=1.0, respectively. When comparing the velocity profiles at the same z/D, increasing rotor height appears to increase the downwash velocity across the entire rotor disc. This observation is expected based on the velocity profiles shown in Fig. 17a. Also, comparing the two velocity profiles at the same rotor height (h/D=1), the peak downwash velocity does not increase substantially with increasing distance below the rotor. Rather, consistent with the OGE behavior, momentum simply transfers from outboard to inboard where low momentum recirculation region exists.

Lateral Axis: Velocity measurements made along 90 and 270 degrees of aircraft azimuth (starboard and port, respectively) at a rotor height of h/D=0.578 are shown in Fig. 19. The color contours represent the horizontal component of velocity and was chosen to show the difference in the nature of flow inside the downwash region. The tandem rotor system has overlapping rotors and the radial location (from the reference center 2 of Fig. 5) where the blade tips meet geometrically is 0.378D. A key difference between the longitudinal and lateral axis is the absence of

14

(a) Non-dimenaionalized using rotor diamter

(b) Non-dimensionalized using rotor height

Figure 17: V_z **variation normal to the rotor plane for two different rotor heights.**
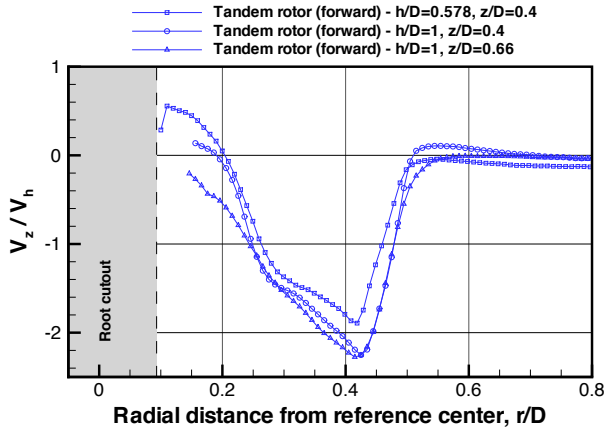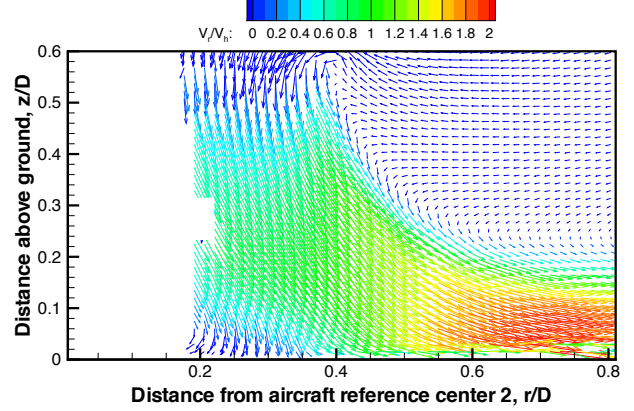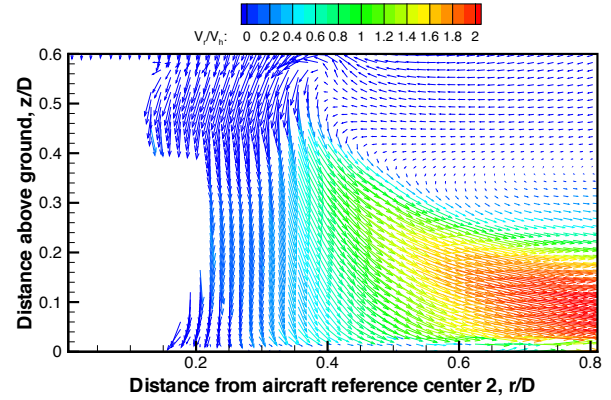

Figure 18: Downwash velocity variation with normal distance at two different rotor heights (h/D=0.578, and 1.0).

the recirculation zone below the rotor in the lateral axis. This is, however, expected because the inflow was provided only by the outboard sections of the blade (where overlapping occurs) that produce positive lift.

The flow field along the lateral axis (90 and 270 deg

(a) Starboard

(b) Port

Figure 19: Flow field comparison between starboard and port sides of the tandem rotor in ground effect at h/D=0.578.

aircraft azimuth) were different. On the starboard side (90 deg aircraft azimuth), the merged flow from both the rotors moved downward before gradually changing its direction away from the aircraft (Fig. 19a). In contrast, the port side showed nearly vertical flow over the entire overlap region (up to r/D=0.378 where blade tips meet) for nearly the entire distance below the rotor up until very close to the ground (Fig. 19b). Vertical and horizontal components of downwash velocity plotted against normal distance from the ground (vertical cut along r/D=0.28 from aircraft center) show this behavior clearly – see Fig. 20. The vertical component of downwash is similar on both sides of the aircraft (Fig. 20a). However, the horizontal component is quite different (Fig. 20b). The port side of the aircraft showed negative V_r values over the entire Region 1 (i.e., for z/D≥0.4). On the other hand, the starboard side showed flow moving away from the aircraft in Region 1 below the rotor plane.

The observed difference in the flow pattern can be explained using the rotational direction of the two rotors, which is counterclockwise for the forward rotor and
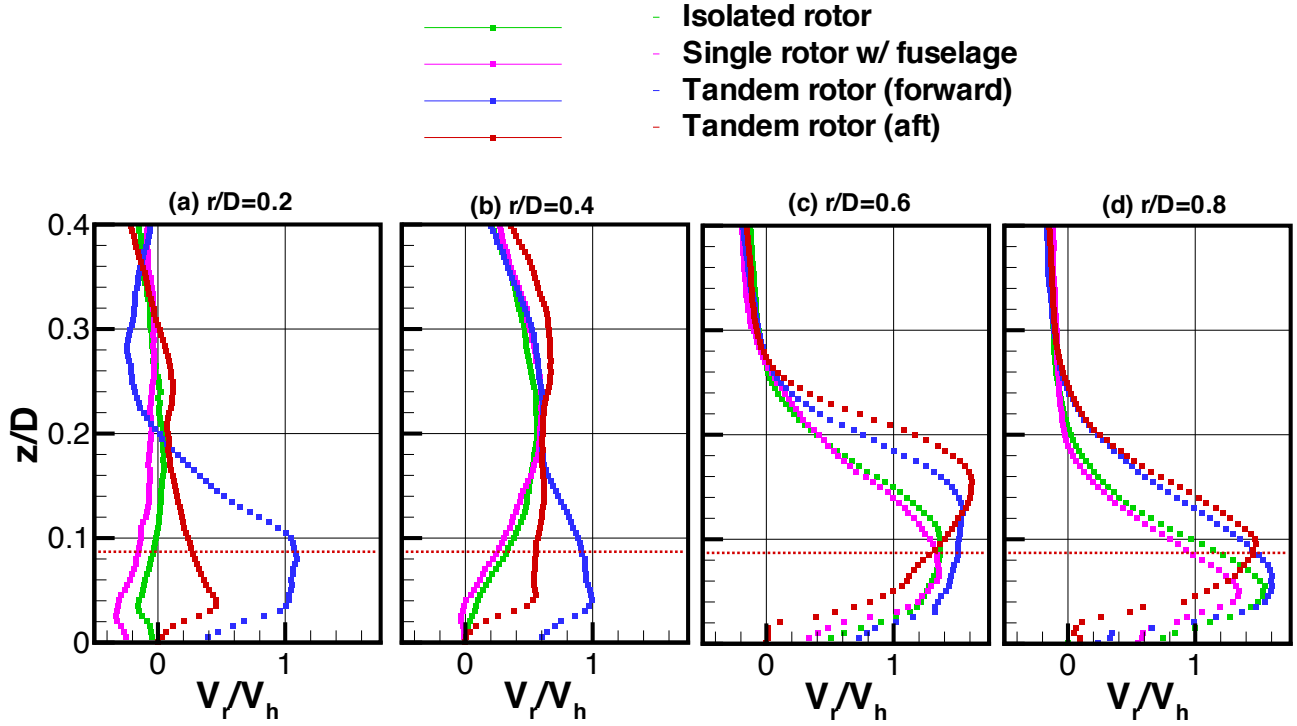
15

Figure 21: Comparison of V_r velocity distribution normal to the ground in the transition region for all rotor configurations (PAXman height=0.09D).

clockwise for the aft rotor. Because the rotors are spinning in opposite direction, the swirl resulting from the combined rotation aids radial outflow away from the aircraft on the starboard side while opposing the outflow on the port side.

Region 2: Transition Region

The transition region exists between the location of maximum wake contraction below the rotor plane and the ground. Radially, the transition region covers the area between the shaft axis (or aircraft center in the case of the lateral planes) and the beginning of Region 3, where the wall jet starts. As mentioned earlier, Region 2 is a key area for personnel safety considerations and brownout initiation. Flow along the longitudinal axis is discussed before analyzing the flow along the lateral axis.

Even though the transition region is analyzed separately from Region 1, the majority of Region 2 still lies under the rotor disc. Consequently, features seen in Region 1 play a role in determining the nature of flow in the transition region. Conversely, flow features present in the transition region can alter flow development in Region 1. This inter-regional interaction can be understood from the changes in the size and shape of the recirculation zone found under the rotor (near the root cutout) in all configurations. To analyze this region effectively, the horizontal velocity

component (V_r) is plotted against normal distance (z/D) from the ground for all rotor configurations at several radial stations in Fig. 21. Velocity fields in Fig. 12 are used to augment Fig. 21 to understand the nature of flow in the transition region. For operations within the rotor outwash, an anthropometric model known as PAXman (Ref. 3) is used to compute forces on personnel. The red dotted line in Fig. 21 represents the height (5 ft, 6 in) of a 6-ft PAXman crouched and leaning while immersed in outwash.

In the cases of isolated single rotors, both with and without fuselage, Fig. 12a and b show that the recirculation region extends to the ground. The presence of the recirculation region results in a stagnation point on the ground. For the isolated rotor IGE (Fig. 12a), the stagnation point is located approximately 0.38D radially away from the shaft axis, meaning that any flow inside this point moves along the ground towards the rotor shaft (r/D=0). Beyond the stagnation point, the flow moves radially away from the rotor. For the single rotor with fuselage (Fig. 12b), the stagnation point occurs at 42%D from the shaft axis. The higher strength vortex near the ground can be inferred from the streamtraces in Fig. 12b as well as by comparing the V_r velocity magnitude exhibited by the green and magenta curves shown in Fig. 21a. The single rotor with fuselage shows larger negative V_r near the ground than the isolated rotor IGE.

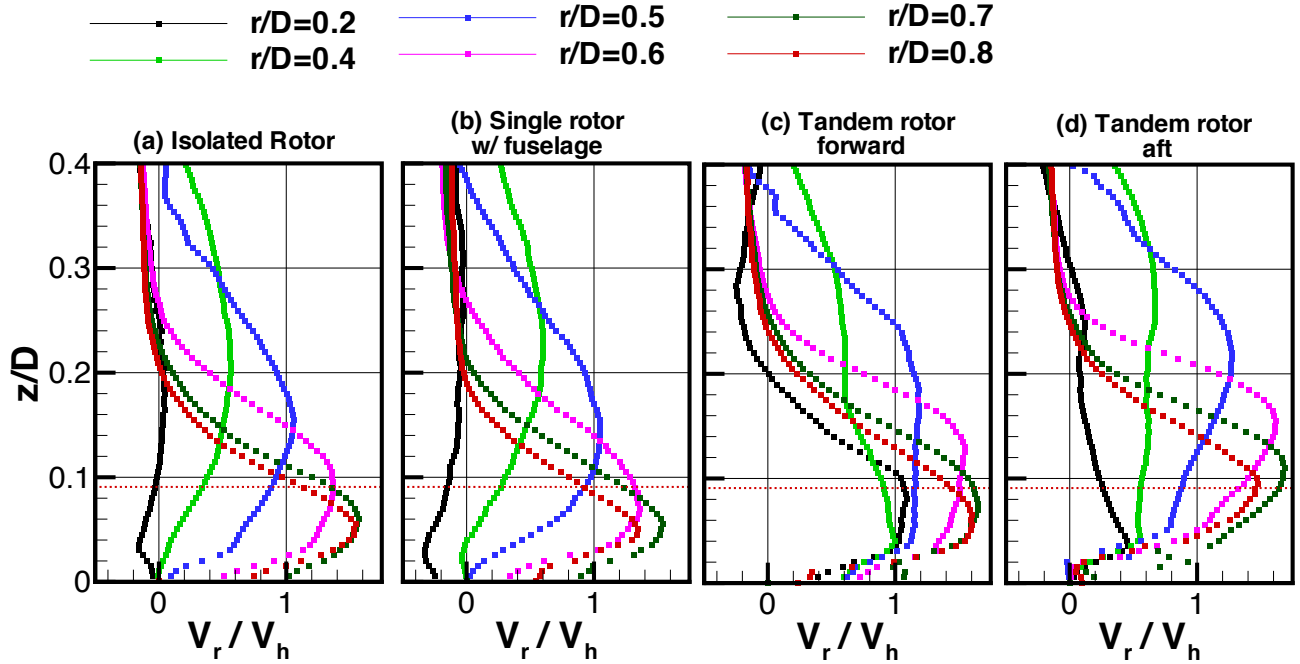A stagnation region beneath an isolated rotor IGE has

Figure 22: V_r **velocity distribution to understand outwash development for all rotor configurations.**

been identified in previous studies. For example, measurements on a model scale isolated single rotor (Ref. 18) showed the stagnation location at 0.25D and 0.2D for a full-scale CH-53E (Ref.22). Tuft flow visualization made beneath a UH-60L helicopter rotor also showed similar characteristics with the stagnation location at about 0.33D from the shaft axis (Ref. 26). The stagnation point and surrounding region (with low momentum) has been suggested as a safe place for personnel.
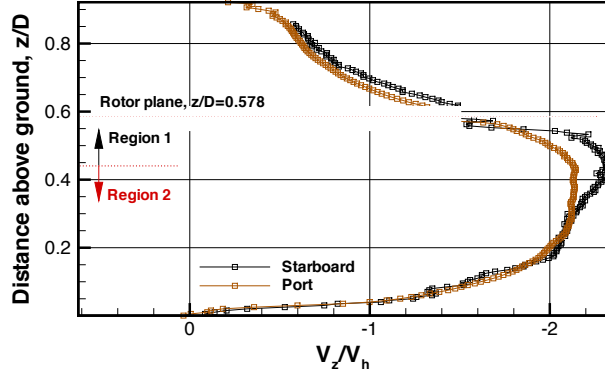
The difference between single rotors and the overlapping rotors of a tandem rotor system in the transition region first appears through the spatial location of the stagnation point. In the case of tandem rotor systems, Fig. 12c shows that the stagnation location for the front rotor moves substantially away above the ground (0.2D) towards the rotor plane because of the flow from the aft rotor. A similar observation was made for the aft rotor. Two observations are important here: 1) the safe zone found beneath the rotor for a single rotor configuration is absent for the tandem rotor system; 2) in front of the forward (or aft) rotor, the flow did not move towards the rotor.

Though a safe zone is absent beneath the rotors of the tandem rotor system, a relatively quiescent flow region may be present beneath the aircraft where fountain-like flow may be expected (see Fig. 2b). However, no measurements were made beneath the aircraft to confirm this supposition. Regarding the second observation, the positive V_r values found near the ground for both the tandem rotor system front and aft rotors (blue and red curves in Fig. 21a and b) are important for pilot visibility issues in
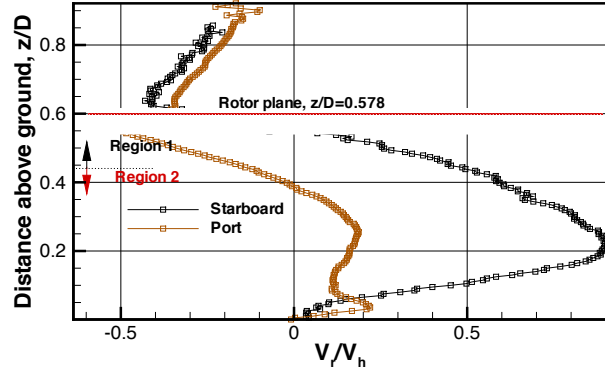
the case of brownout. Also, because of the flow from the other rotor (which is also periodic) more fluctuations in the outwash can be expected. Furthermore, the vertical movement of the stagnation point implies that the size of the recirculation zone in the vertical direction under the rotor was limited to a smaller region - as seen in Fig. 12c and d.

The flow exchange between front and aft rotors for the tandem rotor system not only affects the region of recirculation and the stagnation point, but also the V_r velocity distribution normal to the ground. Figures 21c and d show the V_r distribution outside the rotor disc (two radial stations) plotted against normal distance from the ground for all three rotor configurations. Comparing the isolated rotor IGE and the single rotor with fuselage (IGE), the isolated rotor seems to produce a stronger outwash. The peak measured V_r was 1.42 times the hover induced velocity, while that of the single rotor with fuselage was about 1.35. However, both the front and aft rotors of the tandem rotor system produced higher peak velocity ($\approx$1.6). In addition to the peak velocity magnitude, the normal distance from the ground where the peak occurs is also critical. Higher V_r velocity components away from the ground means that the overturning moments calculated on the PAXman will be higher. The flow is transitioning to become a wall jet in this region, so the velocity profiles are expected to be significantly different at successive radial stations.

At r/D=0.6, (Fig. 21c), flow in front of the forward rotor has the greatest V_r among the other configurations from the ground up to the height of the PAXman. Sur-

(a) Downwash velocity

(b) Outwash velocity

Figure 20: Velocity profiles along the starboard and port sides of the tandem rotor in ground effect (h/D=0.578).
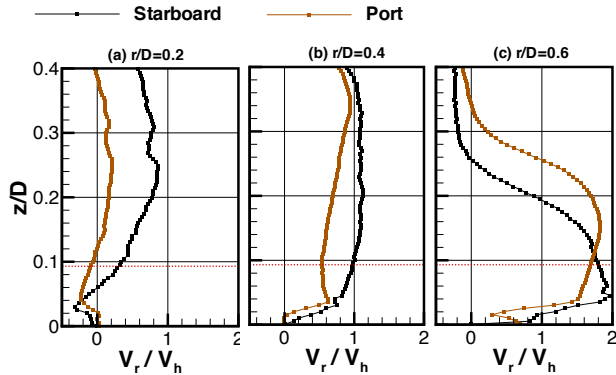

Figure 23: V_r velocity distribution along the lateral axis of the tandem rotor system.

prisingly, the aft rotor showed a more favorable V_r distribution at r/D=0.6 even when compared against the single rotor configurations. Above the height of PAXman, however, the aft rotor showed the highest velocity compared to the other rotors. Both tandem rotor system front and aft rotors showed fuller velocity profiles compared to the single rotors. At r/D=0.8, observations similar to r/D=0.6

can be made except for the expected changes in magnitude of velocities.

The fuller velocity distributions shown in Figs. 21 and 22 are confirmed through the streamtraces drawn from the 75% span location and from the tip of the rotor blade for all three configurations – see Fig. 15. The effect of the front rotor on the aft (and the aft on the front) for the tandem rotor system is evident from the clear deviation of the streamtraces for the tandem rotor system case when compared against single rotor cases as the flow approaches the ground. Streamtraces from the front and aft rotors moved vertically upward to allow flow from the aft and front rotors, respectively. Evidence of flow from one rotor affecting the other confirms that the front-aft plane cannot be considered as a "non-interacting" plane.

To study the development of outwash near the ground in the transition region, Fig. 22 may be used. Here, velocity profiles at various radial stations for each rotor are plotted separately. The highest outwash velocity is seen at r/D=0.7 for all rotor configurations. At r/D=0.8, all configurations show a reduced peak V_r, implying that the decay of the outwash velocity begins between r/D=0.7 and 0.8. The trend of the velocity profiles with r/D in Fig. 22 are indicative of wall jet characteristics, to be discussed in the Outwash/Wall Jet section.

Lateral Axis Figure 20 showed that the starboard side of the aircraft experiences substantially higher outwash velocity near the ground than the port side. Figures 23a to c show the V_r component of velocity at three radial stations. The maximum measured horizontal velocity was about twice the hover induced velocity OGE, as expected based on previous findings (Ref. 31). The objective here is to evaluate the V_r distribution normal to the ground with the perspective of personnel operations near the aircraft.

Inside the rotor disc (i.e., r/D<0.5), the horizontal component of velocity on the port side is always lower than the starboard over the entire transition region below the rotor. Even outside the disc, i.e., at r/D=0.6 and up to the height of PAXman, V_r is higher on the starboard side. However, slightly above the PAXman height (shown as a dotted red line), the port side shows the higher velocity. The trend in terms of the reduced difference in the measured outwash velocity between port and starboard for heights below the PAXman as height increases is captured in full-scale measurements as well (Ref. 31). Though the effect of higher velocity above the PAXman may be less important from a personnel perspective, taller structures and ground equipment in the vicinity might be severely affected by the higher velocity.

The flow along the lateral planes take longer to develop into a wall jet because of the merging of inflow from two rotors. To simplify the analysis, parametric studies in this region will be explored as part of the Region 3 discussion of outwash/wall jet analyses.

Before proceeding with the parametric studies and characterization of the third region, the basic physics of a wall jet is described briefly. Scaling effect, i.e., using model-scale rotors for full-scale rotor analysis, will be discussed as well.

Outwash and Wall Jet Similarities

Developing empirical models based on outwash measurements from all sides of an aircraft require quantification of the following parameters: peak mean outwash velocity (and its decay), location (normal to the ground and various radial distances from the aircraft) of the peak mean outwash velocity, and the outwash velocity profile normal to the ground. However, such empirical models will only be applicable within the bounds of the experimental data. On the other hand, physics-based models that combine and interrelate all the aforementioned variables to the underlying flow mechanisms will be generic and have the potential to be applied to all situations. The challenge for developing such a model comes from understanding the flow phenomena that contribute to the observed characteristics in the flow. Added to this challenge is the complexity introduced through scaling (Reynolds number) when measurements of model-scale rotors are used to understand full-scale rotor phenomena.

In the present study, the discussions in the contracting and transition regions were based on data from a model-scale rotor system. Even though small-scale operating conditions were chosen to match the full-scale measurements (e.g., coefficient of thrust) and the resulting analyses were made using "scaled variables" (e.g., h/D, V_r/V_h etc.) to reflect rotor parameters such as disk loading and rotor diameter, these parameters do not represent the locally dominant phenomena in the flow. The normalized variables facilitate comparison between model-scale and full-scale data, however, such a comparison should only be made when the underlying flow physics (wall jet) is similar between the two scales.

The research conducted on wall jets help significantly in the rotor outwash analysis and scalability studies. Glauert coined the term "wall jet" to represent a jet flowing along the ground with quiescent flow above. Figure 24 shows the assumption made by Glauert, that is, the wall jet is a combination of two basic flows: a boundary layer in the inner layer and a free shear flow (jet from a nozzle) in the outer layer. Above the peak radial velocity, the flow behaves like a free shear flow. For a laminar radial wall jet (and for a turbulent radial wall jet with uniform eddy viscosity), Glauert derived a similarity solution proving that the wall jet profiles remain identical with radial distance provided that the flow parameters are non-dimensionalized using peak radial velocity (at each radial station) and "$z_{1/2}$". The latter variable is the normal dis-
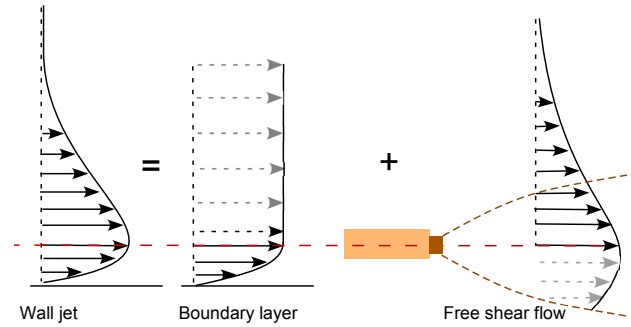

Figure 24: Wall jet velocity profile as a combination of inner boundary layer and outer free jet.

tance above ground where the velocity reaches half the peak value measured at the corresponding radial station. More details on the reasoning behind the choice of $z_{1/2}$ are provided later. Other results of Glauert's analysis include estimation of the growth rate of the jet and the decay rate of the peak radial velocity with distance. Although numerous studies conducted later suggested that there is substantial interaction between the inner viscous flow and the outer inviscid flow, therefore resulting in different coefficients for growth of the jet (and the subsequent decay of the peak velocity), Glauert's fundamental formulation remained the same.

George *et al*. (Ref. 13) carried over the wall jet formulation to rotors for the first time when deriving the equivalent decay for outwash velocity. The difference between the wall jet decay (based on free shear) and the rotor outwash decay (based on induced velocity and free shear) was addressed through modifying the decay coefficients found in jets. These modifications were not simple changes to numerical values but were derived functions of rotor parameters and operating conditions. Ferguson, while developing RoTWash, used George's formulation to represent the decay of rotor outwash velocity. The formulation, when combined with rotor data, allowed Ferguson to determine decay coefficients for rotors. The problem, however, was the limited availability of the data at that time. The high cost of conducting a full-scale rotor outwash survey steered investigations toward small-scale rotor tests. However, scalability studies are needed to ascertain that the physics in full-scale flow are present in model-scale, as well.

Understandably, few scalability studies are available in the literature, considering that the same kind of data are needed for both full-scale and model-scale. Bryan (Ref. 20) compared the outwash from both full-scale and model-scale Boeing VZ-2 proprotor for $r/D = 1$ to 3. Dynamic pressure measured using pitot probes, normalized by disk loading, at various non-dimensionalized radial distances (r/D) showed that the peak mean outwash velocity decay is slightly higher for model-scale rotors
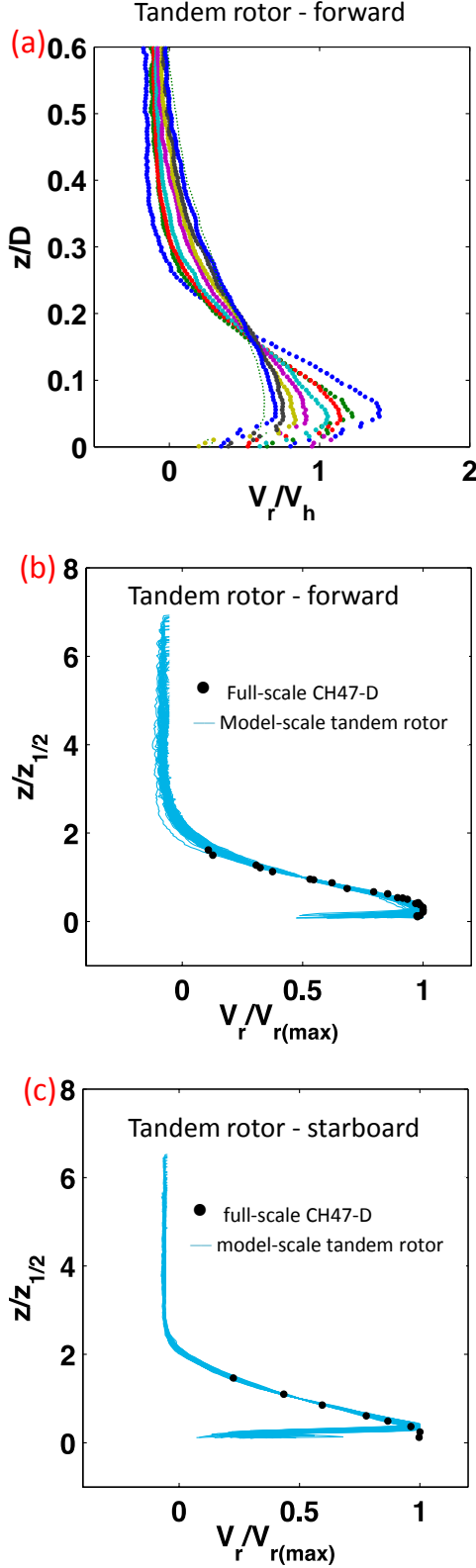
Figure 25: Outwash velocity profiles at various radial distances non-dimensionalized using (a) rotor coordinates, (b) wall jet based similarity variables.

when compared against full-scale. Even though the VZ-2 is a twin rotor system, the measurements were made only when one rotor was operating (essentially a single rotor configuration). Neither the wall jet profile nor the height of the wall jet were compared between model-scale and full-scale.

Wadcock conducted a scalability study (Ref. 25) to evaluate whether model-scale V-22 tilt rotors can be used to replicate the full-scale rotor flow field. Using a 1/40th scale model with the rotor height positioned at an equivalent full-scale wheels-on-ground height, Wadcock reported measurements along a lateral plane of the rotor using untwisted and highly twisted blades for r/D=1.5 to 5. Data were acquired for a wide range of thrust conditions, i.e., at different disk loadings. Despite the wide variation in both twist and planform for blades, when normalized using the peak mean outwash velocity and $z_{1/2}$, model-scale and full-scale data coincided in the outwash velocity distribution. More importantly, the results showed independence of twist when normalized using wall jet variables. Similar conclusions for jets was reported by Ludwig (Ref. 4) using uniform and triangular velocity jets. Such consistency encourages using a jet formulation for rotor outwash analysis. Also, to allow comparison between model- and full-scale peak mean outwash velocity decay, both model-scale and full-scale velocities were normalized by V_h in Ref. 25. Correlation between the model-scale and full-scale rotor outwash was excellent, suggesting that model-scale rotors can be used to replicate the outwash velocity profile and the peak mean outwash velocity decay along the non-interacting lateral plane. Neither the growth of the wall jet nor the scalability studies along the front-aft plane (where flow from the two rotors merge to form a wall jet) were compared between the model- and full-scale rotors in Ref. 25.

The challenge with the tandem rotor system is that, unlike the tilt rotor, the flow from the forward rotor of the tandem rotor system interacts with the aft rotor (and vice versa) as shown in the transition region discussion (and in Fig. 2b). The resulting combined flow is not verified for scalability or evaluated for the applicability of wall jet theory. Also, no reports exists to evaluate the scalability along the lateral axis (starboard-port plane) for the tandem rotor system. The present measurements attempts to address the scalability of the tandem rotor system outwash by comparing all three variables of the wall jets, i.e., wall jet profile, peak velocity decay, and growth rate of the wall jet height for all four aircraft azimuths (both longitudinal and lateral planes) shown in Fig. 5.

Region 3: Outwash

One of the challenges in applying wall jet theory to rotor measurements is locating the "origin" of the wall jet.
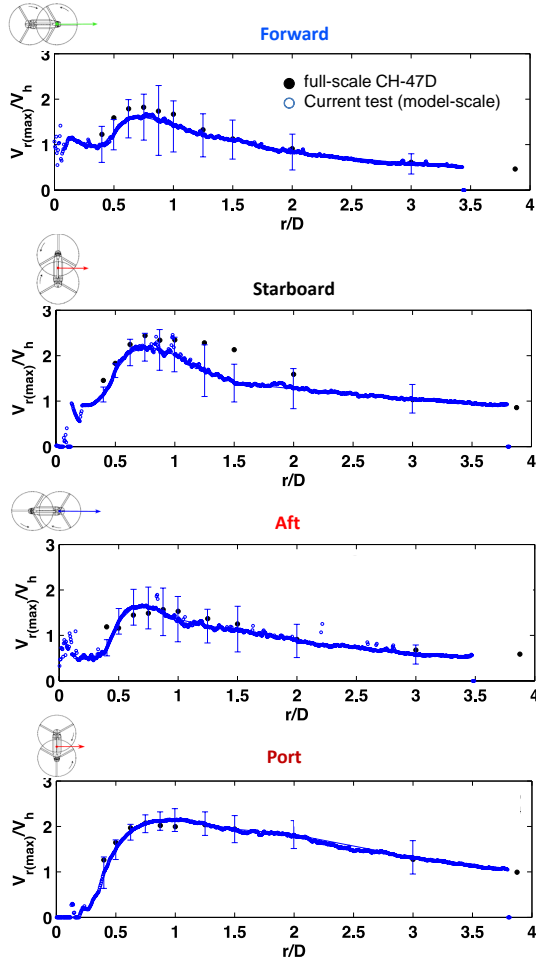
20

Figure 26: Comparison of maximum radial velocity decay in the outwash region between model-scale and full-scale measurements.

The radial location where the peak mean outwash velocity begins decaying (accompanied by a growth in the wall jet width) has been, in the past, assumed as the "origin", where outwash begins exhibiting wall-jet like characteristics.

Velocity profiles normalized using rotor parameters for radial distances greater than r/D=0.75 are shown in Fig. 25a. Using the wall jet parameters, $z_{1/2}$ and peak mean outwash velocity, normalized outwash profiles from r/D=0.7 for the front rotor (0 deg aircraft survey azimuth) are shown in Fig. 25b. A similar plot for 90 deg survey azimuth for r/D>2.0 is shown in Fig. 25c. Because the velocities were normalized with the maximum measured outwash velocity, the entire analysis becomes independent of rotor parameters - allowing a direct comparison with full-scale measurements. Wall jet velocity profiles from multiple radial stations (vertical cuts made on the PIV measurement grid) coalesce into a single profile for both 0 and 90 deg aircraft azimuths independently. Similar results were found for 180 deg and 270 deg azimuths. Full-
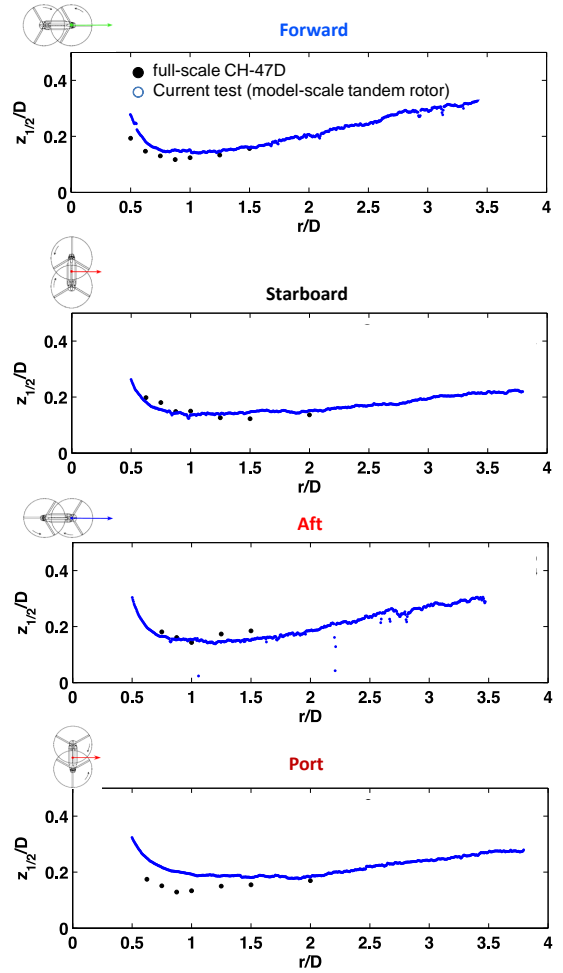

Figure 27: Comparison of $z_{1/2}$ growth between model-scale and full-scale measurements.

scale measurements, treated the same way, collapsed onto the model scale data in Fig. 25, as expected. This result clearly suggests that model-scale and full-scale outwash velocity profiles are scalable in the front-aft and starboard-port planes using simple wall jet parameters, despite the interaction between the two rotors.

Matching wall jet outwash profiles between model- and full-scale alone does not guarantee that the model-scale replicates all the flow phenomena present in the full-scale rotor flow field. For example, velocity profiles would still match even if the turbulence levels are not scaled, i.e., velocity profiles may be self-similar and correlate well with full-scale data, however the growth rate can be different. Only after comparing the decay of peak mean outwash velocity and the growth of $z_{1/2}$ between model- and full-scale (against radial distance), can scalability between model- and full-scale be confirmed.

Figure 26 shows the decay of peak mean outwash velocity with increasing radial distance on all four sides of the aircraft. Full-scale measurements are also plotted for comparison. The bars (σ) represent the model-scale ve-
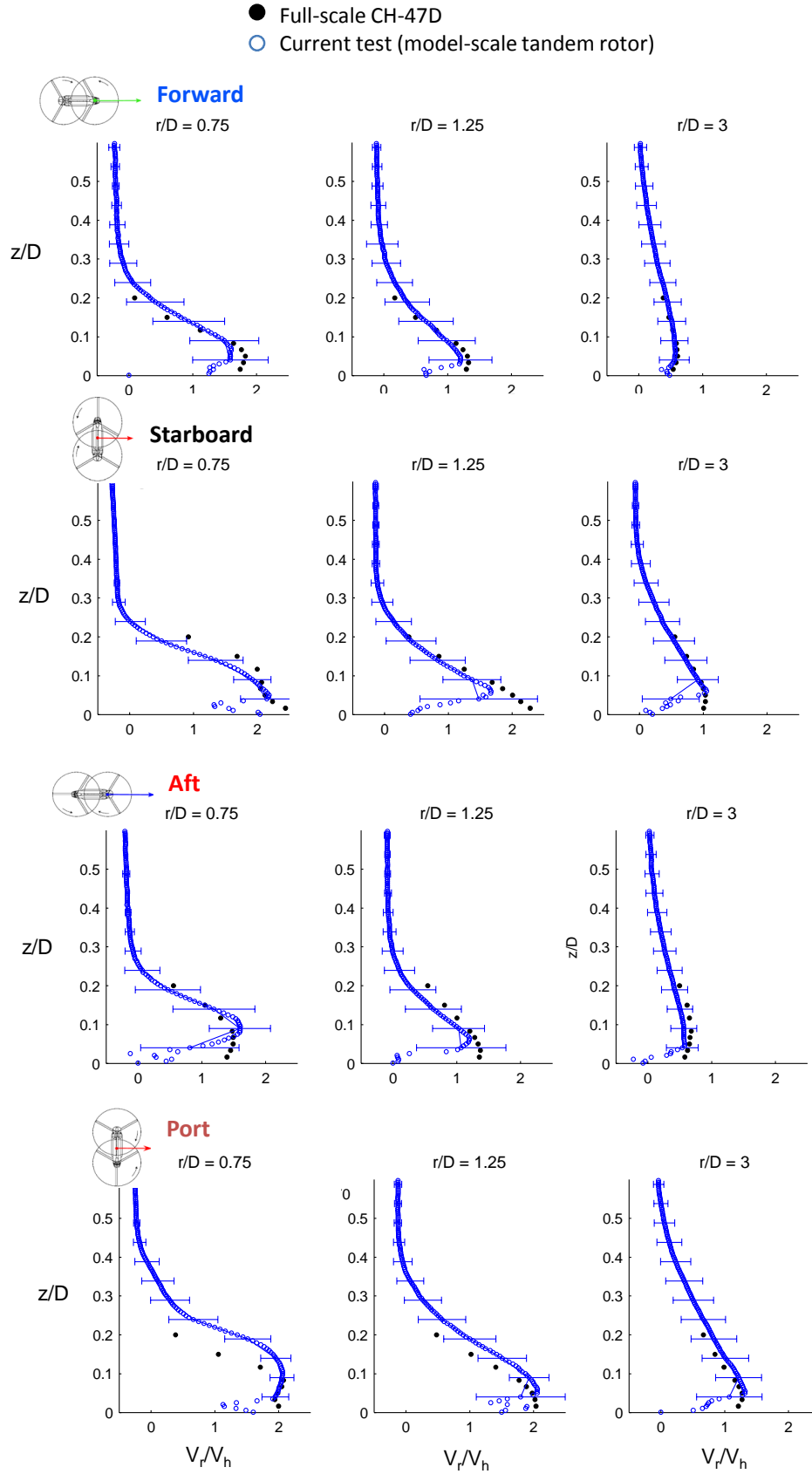
Figure 28: Outwash velocity profiles at various radial distances around the tandem rotor system.

locity variation within the sampling time resulting from the periodic nature of the rotor flow. The bars are only shown at locations corresponding to full-scale measurement locations. Overall the correlation is good for all 4 directions at all radial distances, beginning from inside the rotor disc (transition region) to well outside (r/D>3.5). Normalizing the radial distance with the diameter of the rotor appears to account for the scaling effects. Except for the 90 deg azimuth (starboard side) of the aircraft, especially for r/D between 1.25 and 2.0, all full-scale measurements lie within the periodic variations of model-scale measurements.

The outwash acceleration within the transition region, followed by decay in the wall jet region is captured well. Comparing all four sides of the aircraft, the forward-aft plane produced lower peak outwash velocities ($V_x/V_h \approx$ 1.6) in the near wake (r/D < 1.0) than the starboard-port plane ($V_x/V_h \approx$ 2.2), as expected from the overlapping rotors. The starboard side produced the highest outwash velocity among the four sides of the aircraft.
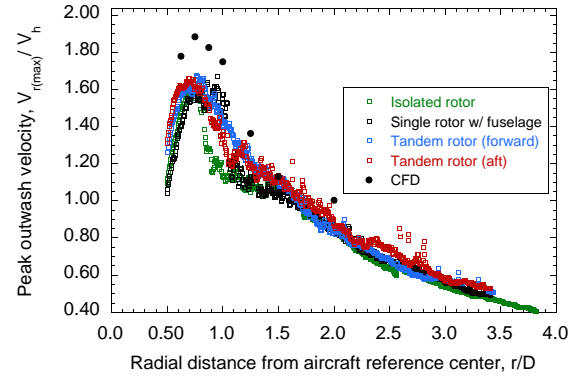
The half-height of the wall jet profile ($z_{1/2}$) versus radial distance is plotted in Fig. 27 for all four sides of the aircraft. For both the forward and aft rotors, the $z_{1/2}$ growth began with the start of outwash velocity decay. However, on the starboard and port sides, up until r/D $\approx$ 0.75, no noticeable growth was found. The growth of $z_{1/2}$ began only after 2 diameters and the growth rate was much slower compared to the forward and aft directions.

Using the three key parameters of wall jet analysis (outwash velocity profile, outwash decay, and $z_{1/2}$ growth) and applying them to both model- and full-scale data, Figs. 25–27 clearly show the data from the model-scale tandem rotors replicate full-scale outwash data when normalized by appropriate rotor and flow variables. The similarity between small- and full-scale outwash holds both when the rotors interact lightly (i.e., forward-aft directions) or heavily (starboard-port directions). With these parameters, the outwash velocity profile at any radial location can be determined. The outwash velocity profiles on all four sides of the tandem rotor system are shown in Fig. 28 for three different radial stations. Again, the bar represents the periodic nature of the model-scale rotor flow (and not uncertainty of the measurements).
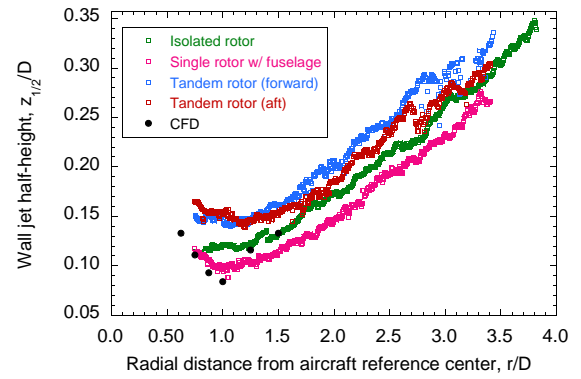
Having established the similarity of model-scale rotor outwash to full-scale, parametric studies were conducted to provide further understanding of the interaction between the rotors, fuselage, and ground.

Parametric Studies

Figure 29 shows the velocity decay and $z_{1/2}$ growth for all rotor configurations (isolated rotor IGE, single rotor with fuselage, and tandem rotor system (front and aft rotors). The results also include CFD predictions. In the wall jet region (i.e., r/D > 0.75), maximum outwash measured for all rotor configurations are of the same order.

(a) Peak mean outwash velocity decay

(b) Wall jet growth

Figure 29: Measured and computed peak mean outwash velocity decay and wall jet growth for various rotor configurations.

However, the wall jet half-height is different for each configuration. Both the front and aft rotors of the tandem rotor system showed larger half-height than the single rotors both with and without fuselage.

Comparison with CFD predictions on isolated single rotor measurements IGE at full-scale Re numbers can only be made up to r/D = 2 because, as mentioned earlier, even after 35 rotor revolutions the starting vortex was still in the calculation (see Fig. 8). A consistent comparison would be against full-scale isolated single rotor IGE. In general, comparisons show that the peak mean outwash velocity predicted by CFD is somewhat higher ($\approx$10-20%) than the measurements at all radial stations, although the trend is captured quite well. The reason for the overprediction is not obvious based on the underpredicted maximum downwash shown earlier. The wall jet half-height is underpredicted around r/D = 1.0, but in reasonable agreement elsewhere. A representative comparison of outwash velocity profiles at r/D = 1.25 is shown in Fig. 30. The CFD peak mean velocity is located closer to the ground and the
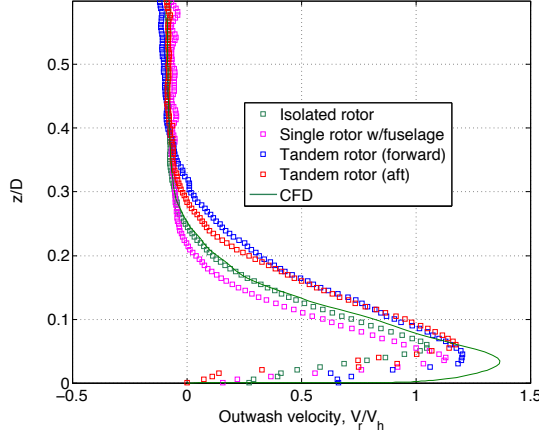
Figure 30: Comparison of velocity profiles for various rotor configurations at r/D=1.25 and h/D=0.578.

boundary layer profile is much fuller, as might be expected due to Re differences.

The height of the wall jet does not correspond to the height above ground where the highest velocity occurs, but rather the height where the velocity is half the highest outwash velocity. The location where the peak mean outwash velocity occurred remained constant almost over the entire measurement range. A value of 0.05D (shown in Table 4) is representative of all rotor configurations.

To understand the peak mean outwash velocity from a PAXman perspective for all four configurations, Fig. 31 shows the outwash radial distribution (for rotor h/D=0.578) at a height equivalent to the full-scale PAXman height (5 ft 6 in) of z/D≈0.09. The forward and aft rotors of the tandem rotor system produced higher outwash than the single rotors (with or without fuselage) near
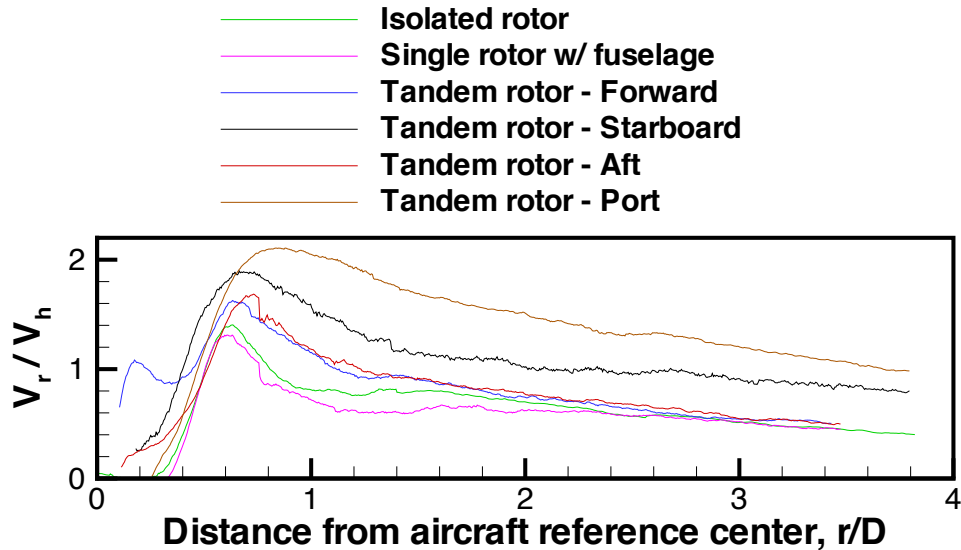
Description	$(z/D)_{max}$	$1\sigma/D$
Isolated rotor	0.05	0.009
Single rotor w/ fuselage	0.038	0.008
Forward (Tandem-rotor)	0.048	0.006
Starboard (Tandem-rotor)	0.054	0.013
Aft (Tandem-rotor)	0.06	0.006
Port (Tandem-rotor)	0.045	0.0157

Note: PAXman height=0.09D

Table 4: Location of Peak mean outwash velocity above ground.

the rotor. As the radial distance increases, they all coalesce into a single curve suggesting tandem rotor systems have higher rate of decay at least in the near wake. For the tandem rotor configuration, up until r/D = 0.65, the starboard side of the rotor produced maximum outwash velocity. However, as radial distance increased, the port side produced the highest velocity. Measurements made for h/D=1 showed similar characteristics at the PAXman height (Fig. 32). Again, these characteristics of maximum outwash velocity relative to all four sides are consistent with full-scale measurements at a ground height of 5 ft reported in Ref. 31. This observation is unexpected based on the direction of rotation of the two rotors and the expected higher velocity on the starboard side resulting from the favorable swirl effects of the two rotors. Furthermore, the outwash velocities along the 90-270 plane of the tandem rotor system remains high (with low decay) even at large radial distances compared with the 0-180 plane.

Figure 32 shows the outwash velocity decay on all four sides of the aircraft for two different rotor heights above the ground plane. Several interesting observations were

Figure 31: V_r velocity at 5ft 6in above the ground plane for all rotor configurations.

made. For the forward and aft directions, the maximum velocity decreased with increasing rotor height close to the rotor (r/D < 0.7). However, as the radial distance increased, the measured peak velocity was higher when the rotor height was increased. A PAXman standing at two different distances from the approaching aircraft will feel different flow behavior. A PAXman standing closer to the rotor landing location will experience higher and higher velocity as the aircraft approaches the ground. However, a PAXman standing farther away will experience reduced velocities with decreasing rotor height. In the literature, the effects of rotor height on peak mean outwash velocity has been a contradictory issue. Some investigations (e.g., Ref 50) report that the height of the Harrier aircraft inversely correlates with the outwash velocity while others (e.g., Ref. 10) suggest the opposite. Discrepancies arise mainly because of the differences in the measurement locations relative to the aircraft.

Along the 90-270 deg plane, the outwash behavior was similar to the outwash in the 0-180 deg plane in the near wake (increase in height reduced the peak outwash velocity). However, in the far wake (r/D>1.5), increase in rotor height also decreased the outwash velocity unlike the 0-180 deg case, implying that a PAXman standing along the 90-270 deg plane at any radial distance will experience increased velocity as the aircraft approaches.

The similarities and differences found between 0-180 and 90-270 deg planes discussed above are observed fully in the full-scale CH-47D measurements (Ref. 31), further validating the similarity of model-scale outwash to represent a full-scale outwash flow field.

While the observations made in the 0-180 deg plane are consistent with wall jet behavior, the observations made in the 90-270 deg plane are not. Therefore, to predict outwash behavior for different rotor heights above the ground, a jet formulation should not be applied to the 90-270 deg plane of a tandem rotor configuration.

Unsteady Flow Mechanisms

The results discussed so far have focused on the mean characteristics of rotor DWOW. Rotor flow is inherently periodic because of the presence of a finite number of blades. Lifting blades produce tip vortices, root vortices, vortex sheets, and pulsation in the inflow (from blade passage), resulting in periodic DWOW. Interaction among these features, as the flow develops, makes the flow field fundamentally unsteady. Such an unsteady flow field has been reported to produce "gusts" on the order of 100% of the mean values in some cases (Refs. 22, 24, 31); therefore, identifying and understanding the underlying unsteady flow phenomena and their influence on DWOW is essential.

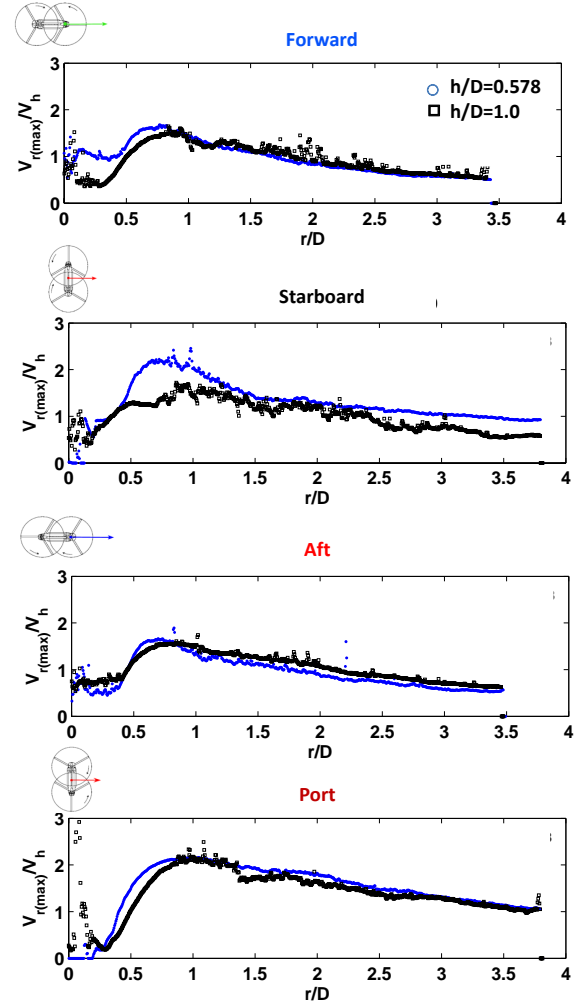Tip vortices are the dominant features of rotor wakes.

Figure 32: Comparison of maximum velocity decay in the Wall jet region for two different rotor heights.

Their influence on rotor performance, vibration, and noise are well documented. In general, tip vortices undergo diffusion where the core size increases and the peak swirl velocity, reduces with increasing time. Several vortex core growth models exist to explain this phenomenon (Refs. 55, 56). However, in ground effect, a vortex filament is known to stretch resulting in a stronger vortex with a smaller core and higher peak swirl velocities (Ref. 57). Stretching counteracts the viscous diffusion process, keeping the vortex core intact much longer compared to OGE conditions.

One of the key phenomenon identified for brownout initiation has been the pairing of tip vortices near the ground (Ref. 14), though the source of the pairing is unknown. Without vortex pairing stretching of the vortex filaments would keep the tip vortices intact and presumably contribute to the outwash unsteadiness even in the far wake. However, tip vortex pairing complicates our un-
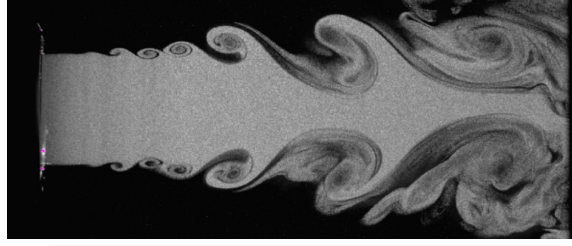
Figure 33: Unsteady flow pheonomena in a free jet (Velocity profiles at 2.5D from nozzle exit).
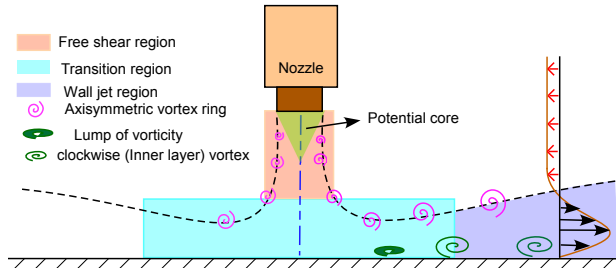

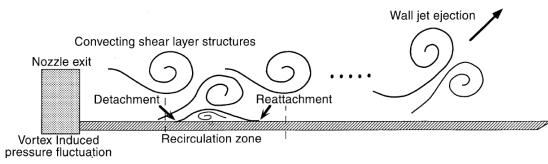**Figure 34: Schematic of the unsteady flow pheonomena for an impinging jet.**

Figure 35: Unsteady flow phenomenon for radial wall jet.

derstanding of the stretching process. Pairing, when followed by uplifting of the tip vortices to re-enter the rotor plane (i.e., recirculation through induced velocity of the rotor) would compress the tip vortex filaments. Compression augments the effects of viscous diffusion, making the vortex core lose its strength quickly. Before proceeding to the discussion of unsteady outwash measurements, the limitations of the data acquisition for both full-scale and model-scale tests are described briefly.

The data acquisition procedure for the full-scale mea-

surements is described in Silva and Riser (Ref. 31) and summarized here to highlight important aspects. All three components of velocity were acquired using ultrasonic anemometers with an internal sampling rate of 160 Hz and a selectable output rate of 4 to 32 Hz. The output rate selected was 20 Hz, meaning that the data were binned (a window of 8 data points). More importantly, the binned data was the median, not the average, of 8 samples. Data were acquired for 30 seconds, resulting in 600 median values that were used to estimate mean, min, max, and 98th percentile of measured velocity. Generally, in the near wake, tip vortices are dominant. In the presence of the ground, they stretch (against diffusion) to retain their coherence for a longer time, making them important features near ground. To capture the Nb/rev periodic variations in the flow field, the Nyquist criterion requires an acquisition frequency of at least $2\times$ (Nb $\times\Omega$) of the rotor. For the forward and aft plane N=3, however, for the starboard-port plane N=6 (overlapping rotors). At 100% rpm (225), an acquisition rate of at least 22.5 and 45 Hz for the front-aft and starboard-port planes, respectively is required. These numbers, when compared against the actual acquisition used in full-scale, suggest that the measurements should be used carefully in the near wake, especially on the starboard-port planes where a higher frequency acquisition is required to capture all phenomena. However, in the wall jet area, where the tip vortices were expected to have merged (with other vortices) and diffused, such high acquisition frequency is not necessary.

The time between two realizations in PIV, used in the present study, corresponds to a frequency of 0.4 Hz, which is very small compared to the rotor rotational frequency (59 Hz). However, because PIV captures the entire flow field at a given instant, the frequency limitation comes from the time integration to estimate the velocity (i.e., time between two laser pulses - 150μs) and not between two realizations. To summarize, the equivalent limitation frequency of PIV used in the present study is about 6500 Hz (i.e., 1/150 μs), which is sufficient for the present analysis.

The remainder of this section addresses two important questions: (1) What is the source of the unsteadiness (of the order of 1 Hz) found in full-scale outwash measurements?, and (2) What is the flow phenomenon that causes pairing of vortices? Previous research on the unsteadiness of impinging jets and wall jets help answer these questions.

Figure 33a shows the unsteady nature of a "steady" jet that has its source in viscous shear (vortex ring instabilities). Laser light sheet flow visualization images and PIV measurements were acquired in free air at a nozzle exit velocity of 50 m/s. Similar measurements were observed for 100 m/s as well. The Re number based on the nozzle diameter of 0.393 in is of the same order as that of tan-
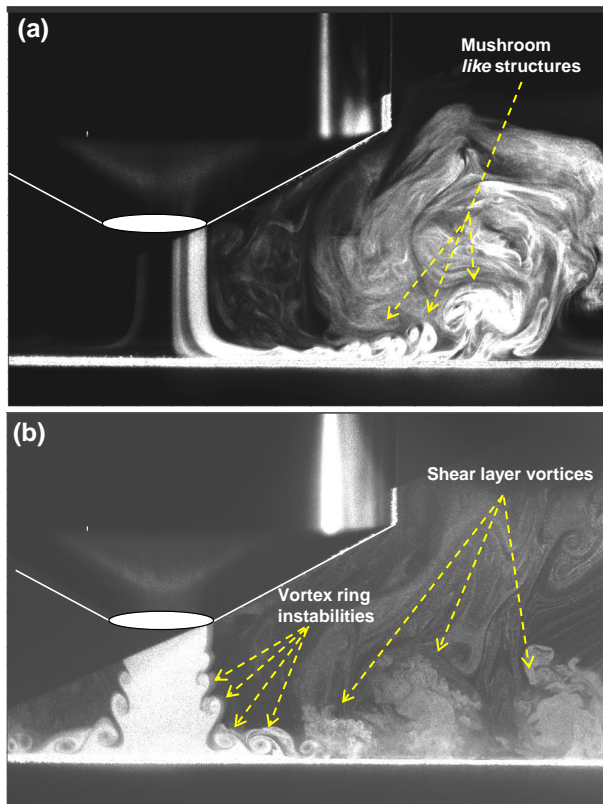
Figure 36: Laser light sheet visualization of the unsteady flow phenomenon for an impinging jet.

dem rotor system measurements (based on rotor diameter) made in the present study. The corresponding mean and fluctuating velocity distributions across the jet 2.5D away from the nozzle exit are shown in Fig. 33b. Two important observations are (1) the minimum fluctuation occurs at the center where the mean velocity is maximum (and the velocity gradient is zero), and (2) the location of the peak rms velocity with respect to the nozzle center (dotted line) corresponds to $z_{1/2}$, where the local velocity is half the peak velocity (dotted line from the peak rms location intersects the mean velocity at Vmax/2). The $z_{1/2}$ location should also correspond to the locus of the center of the shear layer vortices that form the boundary between the jet and the outer quiescent flow. Since the wall jet is a combination of a boundary layer (on the inner layer) and a free shear layer (as the outer layer) as shown in Fig. 24, Glauert used $z_{1/2}$ as a similarity variable to represent the wall jet growth. Applying the $z_{1/2}$ parameter to analyze rotor outwash is a natural extension of free shear flow studies. As shown in Fig. 33a, shear layer vortices can be as large as the nozzle exit and can introduce substantial unsteadiness in free jets, i.e., of the order of 20% of the nozzle exit velocity. Similar results can be expected in the outer layer of the wall jet.

An impinging jet schematic shown in Fig. 34 shows the jet equivalent of a rotor operating IGE for analysis purposes. Even here, shear layer vortices appearing as vortex rings play a role in the flow unsteadiness. Before the jet hits the ground, rms fluctuations of streamwise velocity for impinging jets have shown similar characteristics as free jets, that is, a peak at either edge of the jet (Ref. 51). However, the impingement process introduces additional unsteadiness. Didden & Ho (Ref. 58) suggested that when periodic shear layer vortices pass near the ground, the pressure fluctuations in the inviscid flow create unsteadiness inside the viscous boundary layer. The boundary layer unsteadiness evolves into a lump of clockwise vorticity (opposite sign to the shear layer vortex). Over time, the lump of clockwise vorticity rolls up into a vortex and moves along the ground. The location of the clockwise vorticity is usually between the two shear layer vortices. The resulting clockwise - counterclockwise (shear layer) vortex pair travels downstream before separating from the ground.

To evaluate the applicability of the unsteady flow separation for brownout, Geiser (Ref. 59) conducted experiments on vortex rings. Using a novel experimental setup, vortex rings at pre-defined frequencies were impinged on the ground and measurements were made to understand the vortex ring-boundary layer interaction. The experiments confirmed the theory of Didden & Ho, providing another contributing source for unsteadiness, and brownout: the higher velocity between two opposite-sign paired vortices plays a key role in dust uplift. The interaction of a vortex with the ground, and the resulting opposite sign vortex was found in fixed-wing research (Ref. 52).

Even in the absence of impinging jets, pure wall jets created using flow channels (nozzle) parallel to the ground showed unsteadiness. Key measurements and predictions from Gogineni *et al*. (Refs. 53, 54) show that as flow progresses along the ground, shear layer vortices formed on the upper layer create periodic pressure fluctuations inside the boundary layer. These periodic fluctuations resulted in clockwise-counterclockwise vortex pairs. Consistent with Didden & Ho (Ref. 58), unsteady separation results in wall jet ejection, in the shape of a mushroom. The schematic shown in Fig. 35 is the expected wall jet ejection from Gogineni *et al*. The location where the shear layer instability begins is dependent on Reynolds number.

In the present study, a series of flow visualization experiments was conducted using an impinging jet for a range of Re (very low Re up to the Re of the model-scale rotor test. Representative results are shown in Fig. 36a and b. At very low Re number (Fig. 36a), vortex ring instabilities did not begin until after the jet impinged on the ground. As Re increases, the instability progresses upstream towards the nozzle exit (Fig. 36b). Mushroom-shaped structures (wall jet ejections) and shear layer vortices along the ground expected from jet analyses, are also evident.
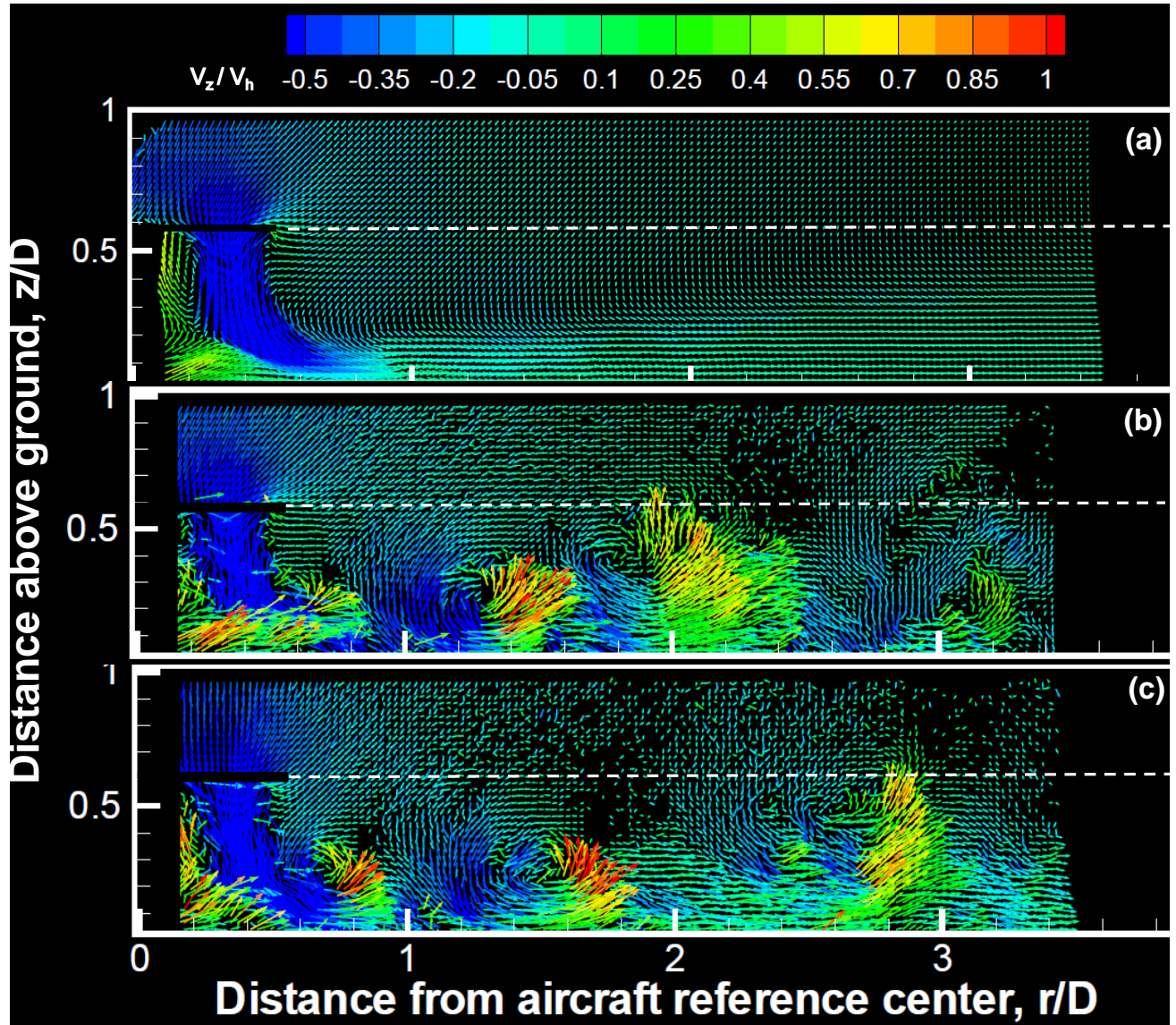
Figure 37: Time averaged and instantaneous flow field of a tandem rotor (forward rotor) IGE (a) Time average, (b)-(c) Instantaneous (h/D=0.578).

Rotor wakes have tip vortices, root vortices, and pulsation from finite number of blades. Figure 1b shows these features, and a comparison with the schematic in Fig. 34 (or the flow visualization pictures of Fig. 36) suggests that tip vortices are of the same sign as the shear layer vortices, and root vortices are of the same sign as the clockwise vortex found inside the jet boundary layer. Tip and root vortices of the rotor wake IGE would augment the effects of shear layer vortices and the clockwise vortex, respectively, because of the same direction of rotation in these pairs. Also, the path followed by root and tip vortices allow them to align with the shear layer and clockwise vorticity, respectively. Basically, the rotor wake is expected to amplify all wall jet characteristics. This may be the reason

why the "wall jet" profile peak estimated by Ferguson using rotor data showed a higher location (from the ground) of $z_{1/2}$ when compared against Glauert's jet (Ref. 34).

To validate a hypothesis that shear layer vortices dominant in impinging jets are playing an equally dominant role in rotor outwash, these vortices must be first located in the rotor outwash. Shear layer vortices are much larger than tip vortices. Figure 37 shows the time-averaged and two instantaneous PIV vector fields for the plane in front of the forward rotor (0 deg aircraft azimuth). Equivalent flow fields for the port-side plane (90 deg aircraft azimuth) are shown in Fig. 38. The dotted line shows the rotor plane.

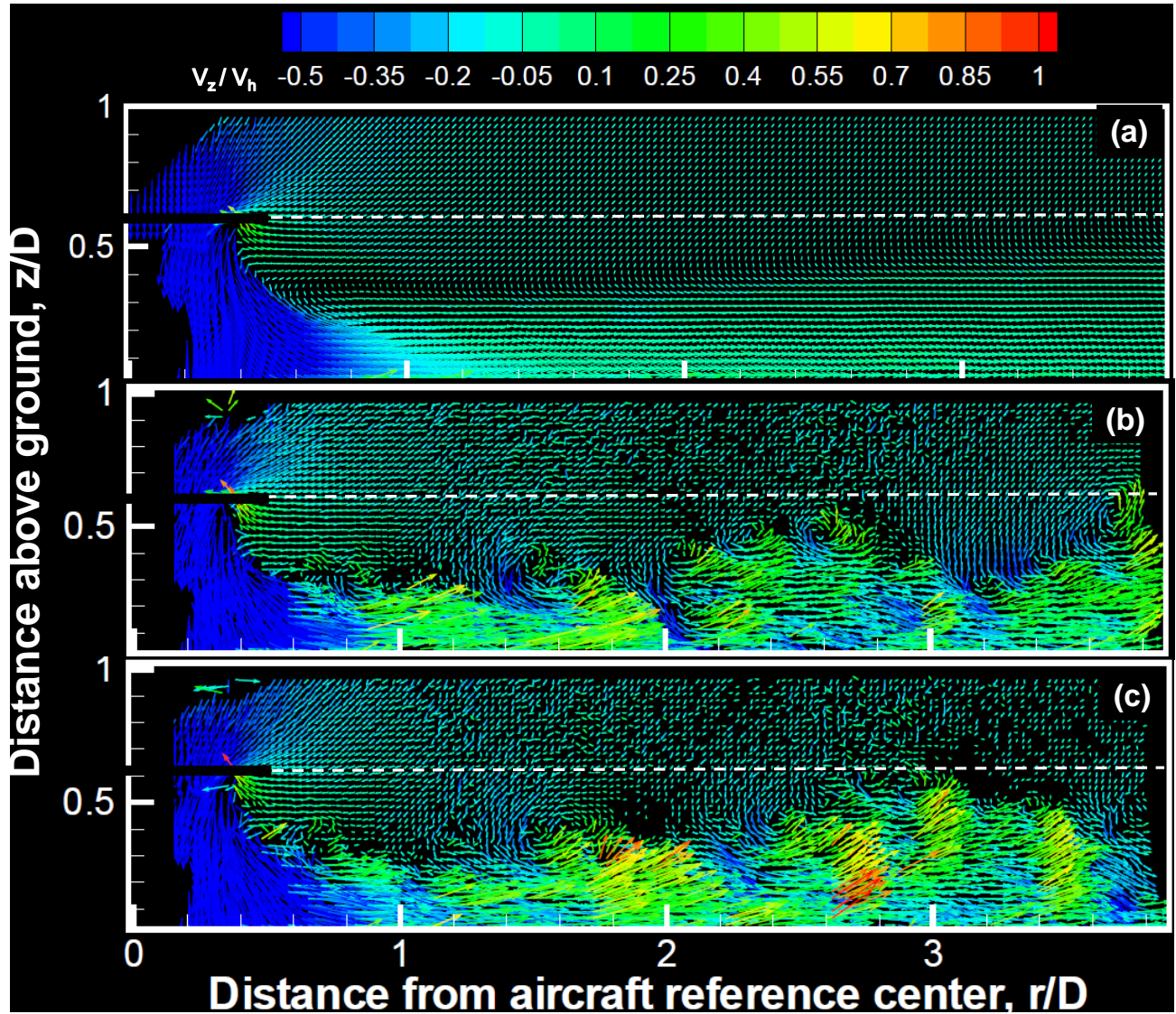Discrete shear layer vortices visible in the 0 deg az-

Figure 38: Time averaged and instantaneous flow field on the port side of tandem-rotor IGE (a) Time average, (b)-(c) Instantaneous (h/D=0.578).

imuth case are not as clearly visible in the 90 deg case. The port plane has twice the number of tip vortices than the forward plane, with half the vortex spacing making vortex merging more likely. Also, the vertical velocity is much lower in the starboard plane compared to the forward plane. A low vertical velocity directly translates to less transfer of momentum from the wall jet to the outer quiescent flow, which explains the lower decay of the measured outwash velocity along the starboard-port plane observed earlier in Figs. 31 and 28. More importantly, the difference between the quiescent average flow field and the feature-filled instantaneous flow fields should be noted.

The average and instantaneous images of Figs. 37 and 38 were created by plotting every 6th vector in each direc-

tion and judiciously adjusting the vector length to bring out the shear layer vortex. The shear layer vortices extend vertically up to the rotor plane (z/D=0.578), much larger in size compared to the typical tip vortex trailing from a rotor blade. Also, the large shear layer vortices house many tip and root vortices – see the close up view of one of the shear layer vortices shown in Fig. 39.

The rms of the outwash velocity measured at r/D=0.75 in front of the forward rotor is shown in Fig. 40. Similar to the rms velocities for the free jet flow shown in Fig. 33, the outer layer of the wall jet near the rotor also shows similar characteristics, i.e., maximum rms occurs at $z_{1/2}$ location of the wall jet. At this location, the velocity fluctuations are as high as the local mean velocity (similar to the observation made in full-scale studies (Ref. 31)). Also, the
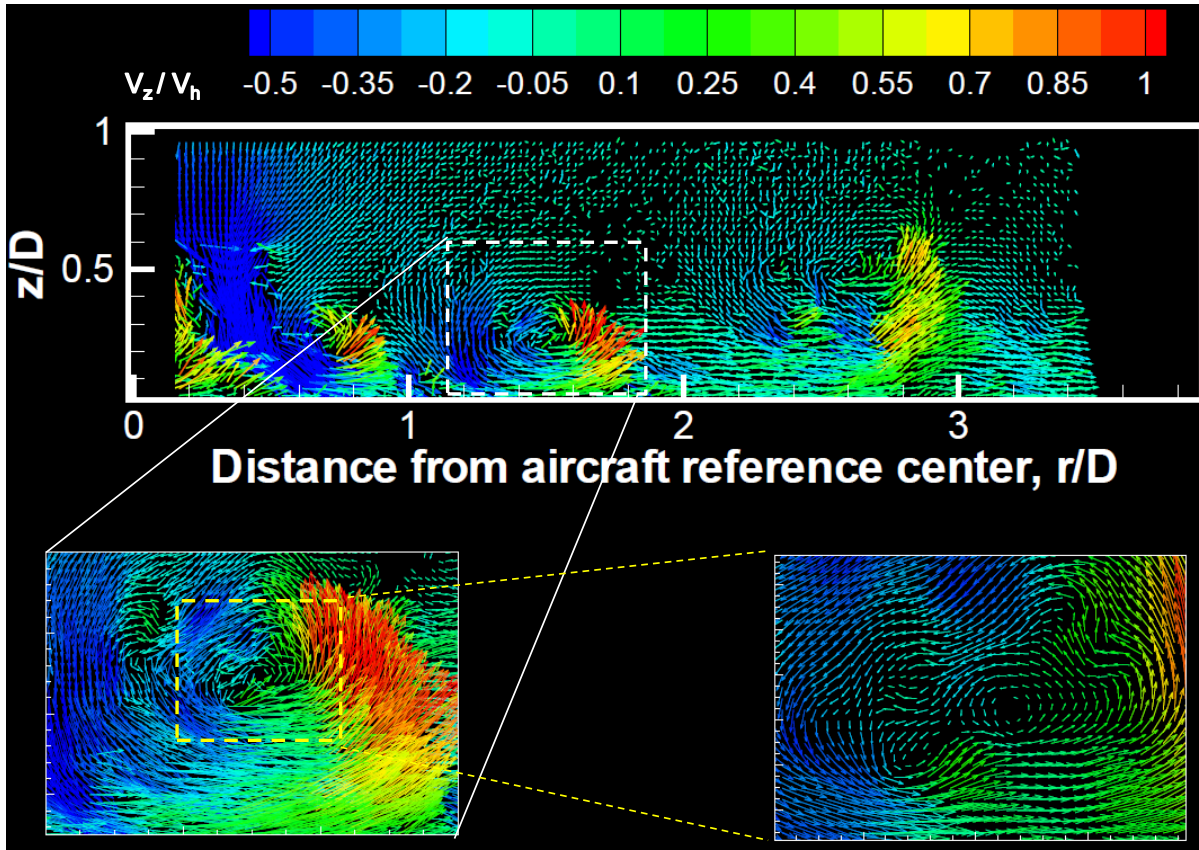
29

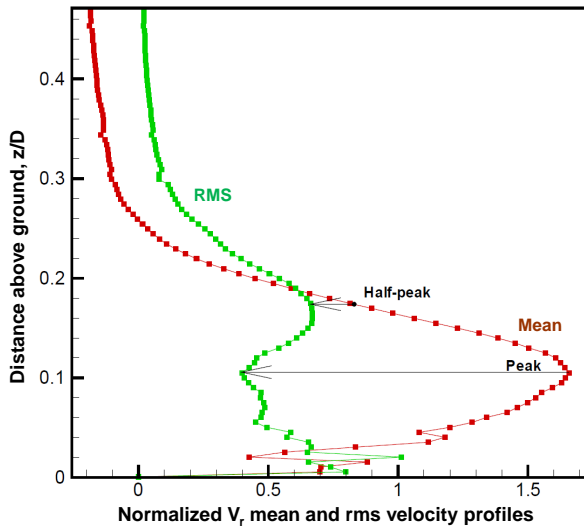**Figure 39: Shear layer vortices and tip vortices in the wall jet.**

Figure 40: Outwash velocity - mean and rms at r/D = 0.75 for the tandem rotor (forward rotor).

rms is at its minimum when the velocity is maximum, a favorable effect for PAXman.

The full-scale rotor observation of low frequency fluctuation may come from these low-frequency, large-scale shear layer vortices. Based on the interval of the shear layer vortices and the average local outwash velocity, flow field oscillations of about 8 Hz result can be inferred from the PIV measurements. The measured 8 Hz is not related to any rotor frequencies and appears independent of the rotor operating conditions. Preliminary single probe hot-wire measurements made on the model-scale tandem rotor (forward) at the same operating conditions confirmed the presence of 8 Hz flow oscillations. More detailed hot-wire measurements are planned for the future. Although model-scale measurements did not capture the full-scale 1 Hz oscillation, model-scale measurements confirm the presence of low frequency velocity oscillations in the tandem rotor flow field. The difference between the model- and full-scale may be attributed to the binning (8 sample) used in the full-scale tests.

The vortex merging process seen in Refs. 11 and 14 may be a result of these shear layer vortices traveling with the speed of the local velocity. The presence of a shear layer vortex may push the tip vortex upward normal to the surface while the tip vortex from the following blade goes
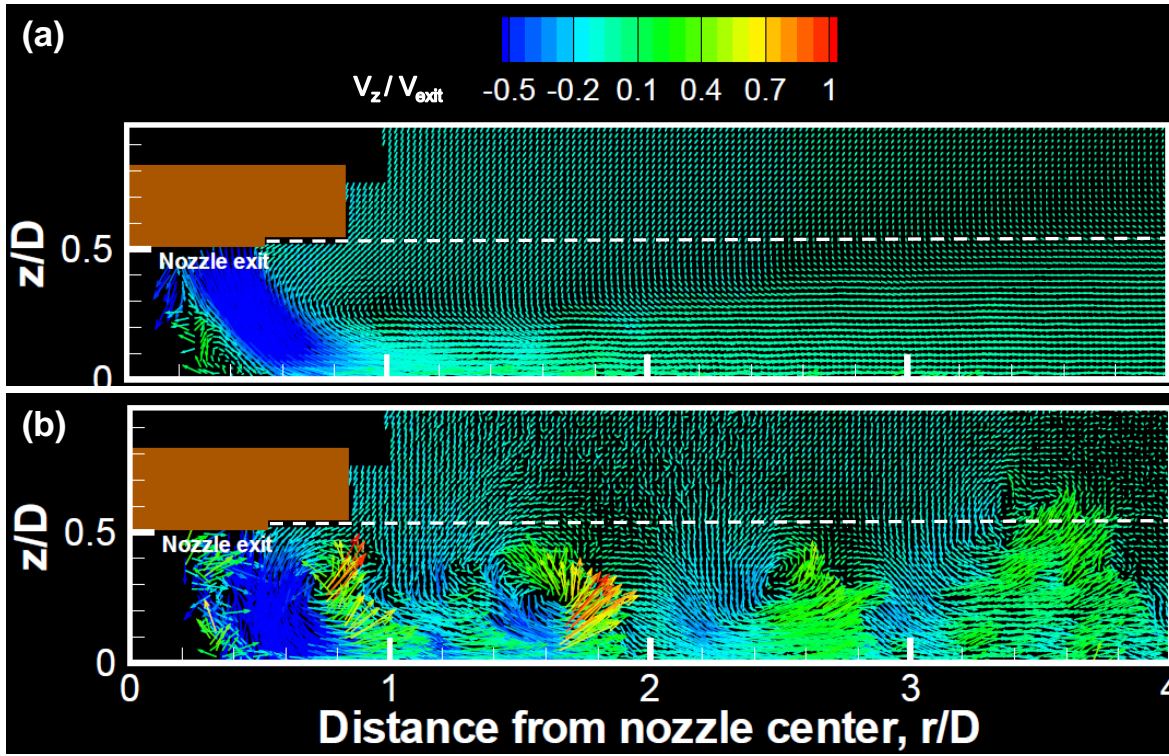
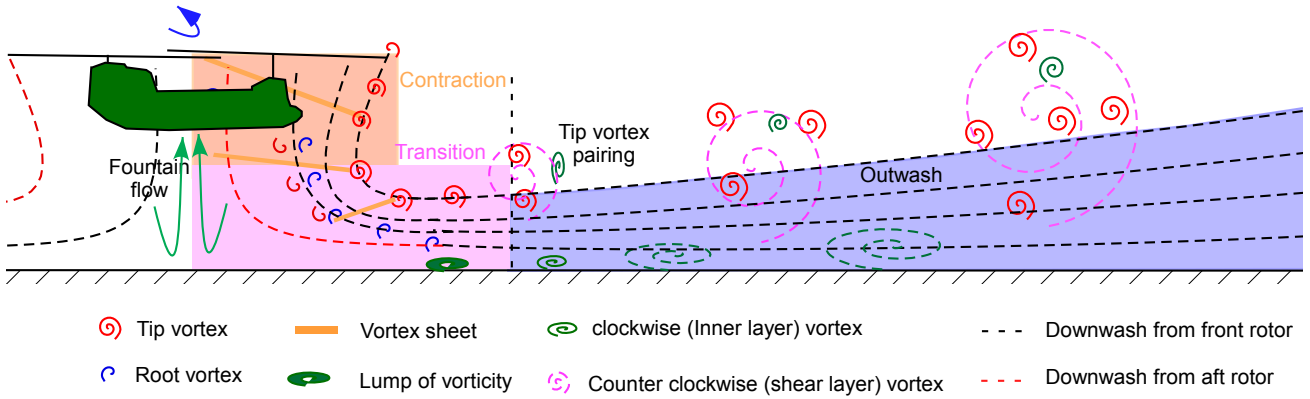**Figure 41: Average and instantaneous flow field from a large nozzle in the presence of the ground.**

Figure 42: Summary of unsteady flow phenomenon in tandem rotor wake.

under the preceding tip vortex. Similar instantaneous flow field measurements made on a large nozzle (with triangular velocity distribution like the one found in Ref. 4) in the presence of the ground is shown in Fig. 41. Flow from the large nozzle, which does not produce tip or root vortices like a rotor, shows identical large-scale vortices as those found in a rotor outwash flow field. Comparison between the two flow fields (Fig. 37 and 41) along with the smaller nozzle flow visualization (Fig. 36) suggests that shear layer vortices play a dominant role in outwash and in dust/debris upliftment (brownout) even in the absence

of tip/root vortices from a rotor blade. In the brownout report by Wong & Tanner (Ref. 28), columns of dust were thrown above the ground away from the full-scale rotor, possibly by the shear layer vortices. Figure 42 summarizes all the unsteady flow phenomenon that have been reported earlier through rotor studies and from the present study on the tandem rotor system.

Conclusions

A series of experiments were conducted to identify and understand various flow phenomena contributing to tandem rotor downwash and outwash. To simplify the problem, flow field measurements were carried out on a single isolated rotor IGE, followed by single rotor with fuselage, and then a complete tandem rotor system model with overlapping rotors. A single isolated rotor OGE served as the baseline configuration. To augment the measurements, especially to understand the unsteady effects, flow field measurements were conducted on jets of different sizes as well. The effect of rotor height on the downwash/outwash was also studied.

Rotor flow fields were divided into 4 regions for fundamental investigation of which the following three regions were analyzed: Contraction, Transition, and Wall Jet/Outwash.

Scaling effects were evaluated by comparing the present model-scale measurements with full-scale measurements in terms of observations, trends and flow variables such as downwash and outwash velocities after normalizing with rotor and/or wall jet variables. Following are the specific conclusions derived from the present study.

OGE: An alternative approach was provided to estimate the induced velocity in hover out of ground effect for realistic rotors (non-uniform inflow). The experimentally measured average V_z value far from the rotor plane was $1.5 \times V_h$ compared to $2 \times V_h$ predicted by momentum theory. Even in the absence of the ground, a low momentum recirculation region was found below the rotor plane (near the root cut out).

CFD Application: Applying high-fidelity CFD to the downwash/outwash problem is a substantial challenge. Computational expense, boundary conditions, turbulence modeling, flow unsteadiness, and the large number of rotor revolutions required to stabilize the flowfield and predict outwash out to 4 rotor diameters all contribute to the challenge. High-fidelity simulations for generating an outwash data set is currently not practical and requires further research.

Configuration Effects:

1. A stagnation location that would facilitate personnel placement was found under the rotor at the r/D=0.38 and 0.42 for an isolated rotor and single rotor with fuselage, respectively. A stagnation location at the ground beneath the rotor was not found for the tandem rotor system.

2. In the wake contraction and transition region, the vertical component of velocity was of the same order for both starboard and port side for the tandem rotor system. However, the horizontal component was much higher on the starboard side than the port side. This can be explained by the direction of rotation of the two rotors relative to the fuselage and the resulting swirl flow.

3. The horizontal component of velocity for both the tandem rotor systems (front and aft) was higher in the transition region than for single rotors with or without fuselage. This result is expected because of the flow contribution from the other rotor, which suggests that the flow in front of the tandem rotor system forward and aft rotors cannot be assumed "non-interactional", at least near the rotor. As radial distance increased, however, the outwash velocities from all configurations collapsed within the periodic variation of the measurements.

4. Outwash velocity profiles were fuller for both tandem rotor system front and aft rotor compared with single rotors with or without fuselage.

5. Peak mean outwash velocity decay began at r/D=0.75 for single rotors (with and without fuselage) and for the tandem rotor system front and aft rotors. The growth of the wall jet width ($z_{1/2}$) also began near r/D=0.75 for these configurations. However, along the 90-270 deg plane, wall jet characteristics ($z_{1/2}$ growth) of the tandem rotor system began near r/D>2.0.

Scaling Studies:

1. All three characteristics of the wall jet, i.e., outwash velocity profile, peak mean outwash velocity, and $z_{1/2}$ growth on all four sides of the model-scale tandem rotor system correlated well with full-scale measurement.

2. Increased rotor height above the ground increased maximum downwash velocity measured below the rotor (at maximum contraction). The location where maximum wake contraction occurred below the rotor, when normalized with rotor height, remained at 30%(h/D).

3. Increasing rotor height above the ground decreases the outwash velocity near the rotor for all 4 sides of the aircraft. However, for r/D> 1D, the peak mean outwash velocity increased with increasing rotor height for the aircraft longitudinal axis. The lateral axis decreased outwash velocity at all radial distances for increased rotor height. The data from the full-scale CH-47D exhibited similar behavior. Although a wall jet analogy is appropriate for the longitudinal plane, the same analogy cannot be applied to the flow in the lateral plane.

4. The peak mean outwash velocity was found to be the highest along the 90 deg (starboard) azimuth near the rotor compared to the other 3 sides of the aircraft. However, farther out from the rotor, the 270 deg (port side) showed higher outwash velocity than 90 deg. These characteristics are consistent with full-scale CH-47D data.

5. CFD predictions show higher peak outwash velocities (10-20%) at all radial stations when compared against equivalent model-scale isolated rotor IGE. The computed peak velocities are located closer to the ground than the model-scale data.

Unsteady Effects:

1. Model-scale outwash velocity measurements clearly showed the presence of a series of large-scale shear layer vortices. These vortices were as high as the rotor height above the ground, transferring momentum from the wall jet to the outer layer. The distribution of outwash rms velocities on the outer layer showed similar characteristics to that of a free shear layer, consistent with the presence of shear layer vortices.

2. The location and distribution of shear layer vortices over the measured 3.8D radial distance were different for forward-aft and starboard-port planes. Along the forward-aft plane, the shear layer vortices are more discrete and transferred more momentum vertically (higher V_z velocity) compared to the starboard-port azimuth plane. This explains the reason for the higher velocities observed along in the lateral plane over large radial distances.

3. The presence of large-scale shear layer vortices in a jet, similar to those found in the model-scale tandem rotor system flow fields suggest that along with tip vortices, shear layer vortices play a significant role in outwash and brownout.

4. The shear layer vortices produced an 8 Hz oscillation in the model-scale flow field. These vortices may be the cause of low frequency oscillations observed in full-scale measurements.

Recommendations for Future DWOW Measurements:

Full-scale

1. Increase data output rate to capture the periodicity (and the associated unsteadiness) of the rotor wake

2. Increase vertical extent of survey to assess impact of expanding unsteady shear-layer vortices

3. Investigate use of non-intrusive velocimetry techniques to survey region beneath hovering helicopters

Model-scale

1. DWOW of various rotor configurations for varying rotor heights above the ground

2. Measure DWOW of tandem rotor configurations for varying amounts of rotor overlap.

3. Acquire detailed hot-wire measurements to capture high and low frequency oscillations present in the tandem rotor flow field.

Acknowledgements

References

[1] Velkoff, H. and Sheppard, A., "The Utilization of Helicopter Technology in the Prevention of Frost in Orange Groves," 11th European Rotorcraft Forum, London, England, September 10–13, 1985.

[2] Schane, LT.C. W. P., "Effects of Downwash Upon Man," U.S. Army Aeromedical Research Unit, Fort Rucker, AL, Report No. 68-3, November 1967.

[3] Preston, J. R., Troutman, S., Keen, E., Silva, M., Whitman, N., Calvert, M., Cardamone, M., Moulton, M., and Ferguson, S. W., "Rotorwash Operational Footprint Modeling, U.S. Army RDECOM Technical Report RDMR-AF-14-02, July 2014

[4] Ludwig, G. R. and Brady, W. G., "Theoretical and Experimental Studies of Impinging Uniform and Non-uniform Jets," TRECOM Technical Report 64-42, U. S. Army Transportation Research Command, Fort Eustis, VA, August 1964.

[5] Kuhn, R. E., "An Investigation to Determine Conditions Under Which Downwash From VTOL Aircraft Will Start Surface Erosion from Various Types of Terrain," NASA TN D-56, September 1959.

[6] Hrycak, P., Lee, D. T. and Gauntner, J. W., "Experimental Flow Characteristics of A Single Turbulent Jet Impinging on a Flat Plate," NASA TN D-5690, March 1970.

[7]Glauert, M.B., "The Wall Jet," *Journal of Fluid Mechanics*, Vol. 1, Part 6, December 1956, pp. 625-643.

[8]Spalart, P. R., "On the Flow Field Induced by a Hovering Rotor or a Static Jet," *Journal of Fluid Mechanics*, Vol. 701, May 2012, pp. 473-481.

[9]Morse, A., "VTOL Downwash Impingment Study Summary Report," TCREC Technical Report 61-37, U. S. Army Transportation Research Command, Ft. Eustis, VA, August 1961.

[10]Meyerhoff, C., "Navy Developmental Test (DT-IIA) of The MV-22 Aircraft Contributory Test Report: Rotor Downwash," Naval Air Test Center Technical Report ACS-CR-90-04, SY71A, Summer 1990.

[11]Lee, T. E., Leishman, J. G. and Ramasamy, M., "Fluid Dynamics of Interacting Blade Tip Vortices with a Ground Plane," *Journal of the American Helicopter Society*, Vol. 55, No. 2, pp. 022005-1-16, April 2010.

[12]Miller, P. and Wilson, M., "Wall Jets Created By Single and Twin High Pressure Jet Impingement," *Aeronautical Journal*, pp. 87–100, March 1993.

[13]George, M., Kisielowski. E. and Douglas, D. S., "Investigation of the Downwash Environment Generated by V/STOL Aircraft Operating in Ground Effect," US-AAVLABS Technical Report 68-52, July 1968.

[14]Johnson, B. S., Leishman, J. G. and Sydney, A., " Investigation of Sediment Entrainment Using Dual-Phase, High-Speed Particle Image Velocimetry," *Journal of the American Helicopter Society*, Vol. 55, No. 4, October 2010.

[15]Milluzzo, J. and Leishman, J. G., "Assessment of Rotorcraft Brownout Severity in Terms of Rotor Design Parameters," *Journal of the American Helicopter Society*, Vol. 55, No. 3, July 2010, pp. 032009-1 – 032009-9.

[16]Knight, M. and Hefner, R. A., "Static Thrust Analysis of the Lifting Airscrew," NACA TN 2220, November 1950.

[17]Taylor, M. K., "A Balsa-Dust Technique for Air-Flow Visualization And Its Application To Flow Through Model Helicopter Rotors In Static Thrust," NACA TN 2220, November 1950.

[18]Fradenburgh, E. A., "Flow Field Measurements for a Hovering Rotor Near the Ground," American Helicopter Society Fifth Annual Western Forum, Los Angeles, CA, September 25–26, 1958.

[19]Bolanovich, M. and Marks, M. D., "Experimental Downwash Velocity, Static Pressure, and Temperature Distributions in Ground Effect for a 75-ft Jet Driven Rotor," *Journal of the American Helicopter Society*, Vol. 4, No. 2, April 1959, pp. 22–36.

[20]Bryan, T. O. "Considerations of the Effect of VTOL Downwash on the Ground Environment," NASA Conference on V/STOL Aircraft, Hampton, VA, January 1960, pp. 261–268.

[21]Newsom, W. A. and Totsi, L. P., "Slipstream Flow Around Several Tilt-Wing VTOL Aircraft Models Operating Near Ground," NASA TN D-1382, September 1962.

[22]Harris, D. J. and Simpson, R. D., "Downwash Evaluation Under the U.S. Army Heavy Lift Helicopter Rotor: Final Report," Naval Air Test Center Technical Report No. SY-17R-76, March 16, 1976.

[23]Light, J. S., "Tip Vortex Geometry of a Hovering Helicopter Rotor in Ground Effect," 45th Annual National Forum of the American Helicopter Society, Boston, MA, May 22–24, 1989.

[24]Lake, R. E. and Clark, W. J., "V-22 Rotor Downwash Survey," NAWCADPAX-98-88-RTR, July1998.

[25]Wadcock, A. J. "Rotor Outwash," Unpublished Presentation made to U. S. Army, Oct 2005.

[26]Wadcock, A. J., Ewing, L. A., Solis, E., Potsdam, M. and Rajagopalan, G., "Rotorcraft Downwash Flow Field Study to Understand the Aerodynamics of Helicopter Brownout," Proceedings of the American Helicopter Society Southwest Region Technical Specialists Meeting, Dallas- FortWorth, TX, October 15–17, 2008.

[27]Nathan, N. D., and Green, R. B., " Measurements of a Rotor Flow in Ground Effect and Visualisation of the Brown-out Phenomenon," Proceedings of the American Helicopter Society 67th Annual Forum, Montreal, Canada, April 29 – May 1, 2008.

[28]Wong, O. D. and Tanner, P. E., " Photogrammetric Measurements of an EH-60L Brownout Cloud ," Proceedings of the American Helicopter Society 66th Annual Forum, Phoenix, AZ, May 11–13, 2010.

[29]Milluzzo, J., Sydney, A. B., Rauleder, J. and Leishman, J. G., " In-Ground-Effect Aerodynamics of Rotors with Different Blade Tips," Proceedings of the American Helicopter Society 66th Annual Forum, Phoenix, AZ, May 11–13, 2010.

[30]Sydney, A. B. and Leishman, J. G., " Understanding Brownout using Near-Wall Dual-Phase Flow Measurements," Proceedings of the American Helicopter Society 67th Annual Forum, Virginia Beach, VA, May 3–5, 2011.

[31]Silva, M. J. and Riser, R., "CH-47D Tandem Rotor Outwash Survey," Proceedings of the American Helicopter Society 67th Annual Forum, Virginia Beach, VA, May 3-5, 2011.

[32]Heyson, H. H., "An Evaluation of Linearized Vortex Theory as Applied to Single and Multiple Rotors Hovering in and out of Ground Effect," NASA TN D-43, September 1959.

[33]George, M., Perlmutter, A. A. and Butler, L., "Downwash Impingement Criteria for VTOL Aircraft," TRECOM Technical Report 64-48, U. S. Army Aviation Material Laboratories, Fort Eustis, VA, July 1964.

[34]Ferguson, S. W., "Rotorwash Analysis Handbook, Volume I Development and Analysis," Federal Aviation Administration, Washington D.C., Technical Report DOT/FAA/RD-93/31, June 1994.

[35]Hohler, D.J., "An Analytical Method of Determining General Downwash Flow Field Parameters for V/STOL Aircraft," AFAPLTR- 66-59, November, 1966.

[36]Migdal, D., Hill, Jr. W. G., Jenkins, R. C. and Siclari, M. J., "VTOL in Ground Effect Flows for Closely Spaced Jets," NASA CR 152321, December 1979.

[37]Watts, A., "V/STOL Downwash Impingement Study - Velocity Estimate," Canadair Aerodynamic Memorandum MAA-284-001, January 1969, Revised April 1971.

[38]Velkoff, H. R., "A Comparative Study of Downwash-Outflow Effects of Various VTOL Configurations as a Factor in the Design Selection Process," 18th European Rotorcraft Forum, Avignon, France, September 15-18, 1992.

[39]Preston, J. R., "VTOL Downwash/Outwash Operational Effects Model, 50th Annual Forum of the American Helicopter Society, Washington D.C., May 11-13, 1994.

[40]Phillips, C., Kim, H. and Brown, R. E., "The Flow Physics of Helicopter Brownout, Proceedings of the 66th Annual AHS Forum, Phoenix, AZ, May 1114, 2010.

[41]Thomas, S., Lakshminarayan, V., K., Kalra, T. S. and Baeder, J. D., "Eulerian-Lagrangian Analysis of Cloud Evolution using CFD Coupled with a Sediment Tracking Algorithm, Proceedings of the 67th Annual AHS Forum, Virginia Beach, VA, May 3-5, 2011.

[42]Zhao, J. and He, C. "Physics-Based Modeling of Viscous Ground Effect for Rotorcraft Applications, Proceedings of the 70th Annual AHS Forum, Montreal, Canada, May 2014.

[43]Hayden, E. W., Abras, J. N. and Silva, M. J., "CH-53K Outwash Modeling Final Report 20131113, CREATE-AV Pilot Project 2013-09, unpublished, Distribution A.

[44]Polsky, S., A. and Wilkinson, C. H., "A Computational Study of Outwash for a Helicopter Operating Near a Vertical Face with Comparison to Experimental Data," AIAA Modeling and Simulation Technologies Conference, Chicago, IL, August 10–13, 2009.

[45]Syal, M. and Leishman, J. G., "Comparisons of Predicted Brownout Dust Clouds with Photogrammetry Measurements," Proceedings of the 67th Annual AHS Forum, Virginia Beach, VA, May 3-5, 2011.

[46]Wachspress, D.A., Whitehouse, G.R., Keller, J.D.,Yu, K., Gilmore, P., Dorsett, M. and McClure, K., "High Fidelity Rotor Aerodynamic Module for Real Time Rotorcraft Flight Simulation," Proceedings of the 65th Annual AHS Forum of the American Helicopter Society, Grapevine, TX, May 27-29, 2009.

[47]Derby, M. D. and Yamauchi, G. K., "Design of 1/48th -Scale Models for Ship/Rotorcraft Interaction Studies," AIAA 2003-3952, 21st Applied Aerodynamics Conference, Orlando, FL, June 2003.

[48]Wissink. A., Jayaraman, B., Datta, A., Sitaraman, J., Potsdam, M., Kamkar, S., Mavriplis, D., Yang, Z., Jain, R., Lim, J. and Strawn, R., "Capability Enhancements in Version 3 of the Helios High-Fidelity Rotorcraft Simulation Code," AIAA paper 2012-713, 50th AIAA Aerospace Sciences Meeting, Nashville, TN, January 9-12, 2012.

[49]Jain, R. K., Lim, J. and Jayaraman, B., "Helios Modular Multi-Solver Approach for Efficient High-Fidelity Simulation of the HART II Rotor," 5th Decennial AHS Aeromechanics Specialists Conference, San Francisco, CA, January 22–24, 2014.

[50]Michaelsen, O. E., "A Comparison of Outflows From a Helicopter, Tilt Wing And Jet Lift Hovering Aircraft," AIAA 71-992, AIAA 8th Annual Meeting and Technology Display, Washington D. C., October 25–28, 1971.

[51]Myszko, M. and Knowles, K., "Development of a Wall Jet from an Impinging Round Turbulent, Compressible Jet," AIAA 94-2327, 25th AIAA Fluid Dynamics Conference, Colorado Springs, CO, June 20–23, 1994.

[52]Harvey, J. K. and Perry, F. J., "Flowfield Produced by Trailing Vortices in the Vicinity of the Ground," *AIAA Journal*, Vol. 9, No. 8, August 1971, pp. 1659–1660.

[53]Gogineni, A. and Shih, C., "Experimental Investigation of the Unsteady Structure of a Transitional Plane Wall Jet" *Experiments in Fluids*, Vol. 23, No. 2, July 1997, pp. 121–129.

[54]Gogineni, A., Visbal, M. and Shih, C., "Phase-Resolved PIV Measurements in a Transitional Plane Wall Jet: A Numerical Comparison" *Experiments in Fluids*, Vol. 27, No. 2, July 1999, pp. 126–136.

[55]Lamb, H., *Hydrodynamics*, 6th ed., Cambridge University Press, Cambridge, 1932, pp. 592–593.

[56]Squire, H. B., "The Growth of a Vortex In Turbulent Flow," *Aeronautical Quarterly*, Vol. 16, August 1965, pp. 302–306.

[57]Ramasamy, M. and Leishman, J. G., "Interdependence of Diffusion and Straining of Helicopter Blade Tip Vortices," *Journal of Aircraft*, Vol. 41, No. 5, September 2004, pp. 1014–1024.

[58]Didden, N. and Ho, C., "Unsteady Separation in a Boundary Layer Produced by an Impinging Jet," *Journal of Fluid Mechanics*, Vol. 160, November 1985, pp. 235–255.

[59]Geiser, J. S., "Effects of Wall Plane Topology on Vortex - Wall Interactions in a Forced Impinging Jet," M. S. Thesis, University of Maryland, 2011.